

Dynamical Evolution of the Mass Function of Globular Star Clusters

S. MICHAEL FALL¹ AND QING ZHANG^{1,2}

`fall@stsci.edu, qzhang@stsci.edu`

ABSTRACT

We present a series of simple, largely analytical models to compute the effects of disruption on the mass function of star clusters. Our calculations include evaporation by two-body relaxation and gravitational shocks and mass loss by stellar evolution. We find that, for a wide variety of initial conditions, the mass function develops a turnover or peak and that, after 12 Gyr, this is remarkably close to the observed peak for globular clusters, at $M_p \approx 2 \times 10^5 M_\odot$. Below the peak, the evolution is dominated by two-body relaxation, and the mass function always develops a tail of the form $\psi(M) = \text{const}$, reflecting that the masses of tidally limited clusters decrease linearly with time just before they are destroyed. This also agrees well with the empirical mass function of globular clusters in the Milky Way. Above the peak, the evolution is dominated by stellar evolution at early times and by gravitational shocks at late times. These processes shift the mass function to lower masses while nearly preserving its shape. The radial variation of the mass function within a galaxy depends on the initial position-velocity distribution of the clusters. We find that some radial anisotropy in the initial velocity distribution, especially when this increases outward, is needed to account for the observed near-uniformity of the mass functions of globular clusters. This may be consistent with the observed near-isotropy of the present velocity distributions because clusters on elongated orbits are preferentially destroyed. These results are based on models with static, spherical galactic potentials. We point out that there would be even more radial mixing of the orbits and hence more uniformity of the mass function if the galactic potentials were time-dependent and/or non-spherical.

Subject headings: celestial mechanics, stellar dynamics — Galaxy: kinematics and dynamics — galaxies: kinematics and dynamics — galaxies: star clusters — globular clusters: general

¹Space Telescope Science Institute, 3700 San Martin Drive, Baltimore, MD 21218

²Department of Physics and Astronomy, Johns Hopkins University, 3400 N. Charles Street, Baltimore, MD 21218

1. Introduction

Globular clusters appear to have a preferred mass scale. Their mass function has a turnover or peak at $M_p \approx 2 \times 10^5 M_\odot$ and a dispersion of only $\sigma(\log M) \approx 0.5$ (Harris 1991). The mass and luminosity functions of globular clusters are often modeled as lognormal functions, although they can also be represented by several broken power laws (McLaughlin 1994). Moreover, globular clusters represent the most numerous gravitationally bound stellar subsystems within the spheroidal components of galaxies (the others being dwarf galaxies). There are relatively few subsystems in galactic spheroids with masses between those of individual stars and globular clusters (i.e., in the range $10^0 \lesssim M \lesssim 10^4 M_\odot$) and between those of globular clusters and the spheroids themselves (i.e., in the range $10^6 \lesssim M \lesssim 10^{10} M_\odot$ for a large galaxy). The preferred mass scale of old globular clusters may be an important clue in understanding their formation and evolution. The corresponding feature in the luminosity function, at $M_V \approx -7.3$, is sometimes used as a distance indicator (e.g., Whitmore 1997).

In contrast, the mass functions of many other types of astronomical objects appear to be scale-free and are often modeled as single power laws. For diffuse and molecular clouds in the Milky Way, the mass function has the form $\psi(M) \propto M^\beta$ with $\beta \approx -2$ over the range $10^{-1} \lesssim M \lesssim 10^6 M_\odot$ (Dickey & Garwood 1989; Solomon & Rivolo 1989). For young star clusters in the disks of normal galaxies (i.e., open clusters), the luminosity functions, which may or may not reflect the mass functions, are power laws, $\phi(L) \propto L^\alpha$ with $\alpha \approx -2$ (Milky Way: van den Bergh & Lafontaine 1984; Large Magellanic Cloud: Elson & Fall 1985; M33: Christian & Schommer 1988). Finally, for the young star clusters formed in interacting and merging galaxies, the luminosity and mass functions also have power-law form, with $\alpha \approx \beta \approx -2$ for $10^4 \lesssim M \lesssim 10^6 M_\odot$ (Whitmore et al. 1999; Zhang & Fall 1999, and references therein³). The last finding is particularly significant because these clusters are often regarded as young globular clusters.

Two explanations have been proposed for the preferred mass scale of old globular clusters. One is that the conditions in ancient galaxies and protogalaxies favored the formation of objects with masses $\sim 10^5$ – $10^6 M_\odot$ but that these conditions no longer prevail in modern galaxies. For example, the minimum mass of newly formed star clusters, set by the Jeans mass of interstellar clouds, will be high when the gas cannot cool efficiently and low when it can, which in turn will depend on the abundances of heavy elements and molecules, the strength of any heat sources, and so forth. These effects may have suppressed the formation of low-mass clusters in the past but not at present (Fall & Rees 1985; Kang et al. 1990). The other explanation for the preferred mass scale of old globular

³Whitmore et al. (1999) found that a double power law with $\alpha_1 = -1.7$ and $\alpha_2 = -2.6$ provided a slightly better fit than a single power law with $\alpha \approx -2$ to the luminosity function of young star clusters in the Antennae galaxies (NGC 4038/9). However, this still contrasts sharply with the luminosity function of old globular clusters. Suggestions that the luminosity and mass functions of the young star clusters in the Antennae might be similar to those of old globular clusters were based on earlier, less sensitive observations, which could not reach beyond the putative turnovers in these functions (Meurer 1995; Fritze-von Alvensleben 1999).

clusters is that they were born with a much wider spectrum of masses that was later modified by the selective destruction of low-mass clusters (Fall & Rees 1977; Gnedin & Ostriker 1997, and references therein). In this case, a power-law mass function might evolve into a lognormal-like mass function (Vesperini 1997, 1998; Baumgardt 1998). This idea is appealing because the masses and sizes of the brightest young clusters in merging galaxies are similar to those of the old globular clusters in the spheroids of galaxies.

Star clusters are relatively weakly bound objects and are vulnerable to disruption by a variety of processes that operate on different timescales. Stellar evolutionary processes remove mass from clusters by a combination of supernovae, stellar winds, and other ejecta. These are effective on both short timescales ($t \lesssim 10^7$ yr), when the clusters or protoclusters are partly gaseous, and on intermediate timescales ($10^7 \lesssim t \lesssim \text{few} \times 10^8$ yr), when the clusters consist entirely of stars. Three stellar dynamical processes remove mass from clusters on long timescales ($t \gtrsim \text{few} \times 10^8$ yr). First, internal relaxation by two-body scattering causes some stars to gain enough energy to escape from the clusters. Second, as clusters orbit around a galaxy, they experience a time-dependent tidal field, which may vary rapidly enough when they pass near the galactic bulge or through the galactic disk that stars in the outer parts of the clusters cannot respond adiabatically. The corresponding changes in the energy of the stars (heating and relaxation) cause some of them to escape. These effects are known respectively as bulge and disk shocks and more generically as gravitational shocks. Third, dynamical friction, the deceleration of clusters induced by the wakes of field stars or dark matter particles behind them, causes the clusters to spiral toward the galactic center, where they may be destroyed by the strong tidal field.

A potentially serious problem with the idea that disruption causes the turnover in the mass function of globular clusters is that the chief disruptive processes operate at different rates in different parts and different types of galaxies (Caputo & Castellani 1984; Chernoff, Kochanek, & Shapiro 1986; Chernoff & Shapiro 1987; Aguilar, Hut, & Ostriker 1988; Gnedin & Ostriker 1997; Murali & Weinberg 1997a,b,c). For example, the rate at which stars escape by two-body relaxation depends on the density of a cluster, which is determined by the tidal field, and hence is higher in the inner parts of galaxies than in the outer parts. The rate at which stars escape by gravitational shocks is also higher in the inner parts of galaxies, both because the orbital periods are shorter there and because the surface density of the disk is higher there. Moreover, disks are absent in elliptical galaxies. Thus, if the mass function were strongly affected by disruptive processes, one might expect its form to depend on radius within a galaxy and to vary from one galaxy to another. This, however, appears to be contradicted by many observations showing that the luminosity function of clusters (a mirror of the mass function when the spread in ages is relatively small) varies little, if at all, within and among galaxies (Harris 1991).

The goal of this paper is to explore the evolution of the mass function of star clusters by a variety of disruptive processes, including evaporation by two-body relaxation and gravitational shocks and mass loss by stellar evolution. We are especially interested in how the mass function is affected by different position-velocity distributions of the clusters, and which of these are compatible

with observations. We formulate this problem in terms of a simple, approximate model that can be solved largely analytically. This clarifies how the mass function is affected by the different disruptive processes and different position-velocity distributions. Our calculations are performed in the context of static, spherical galactic potentials. But we also discuss qualitatively how our results would be affected by time-dependent and non-spherical galactic potentials. The plan for the remainder of the paper is as follows. In Section 2, we specify our model, with the associated assumptions, equations, and parameters. We present the results of our calculations in Section 3, showing the influence of each physical effect on the evolution of the mass function. In Section 4, we compare our results with previous studies, and in Section 5, we summarize our conclusions.

2. Models

We are interested here in the evolution of the mass function of star clusters, defined such that $\psi(M, t)dM$ is the number of clusters with masses between M and $M + dM$ at time t . We assume that the clusters present initially, at $t = 0$, lose mass continuously (smoothing over the escape of individual stars) and that no clusters are created subsequently. Then the mass function must satisfy the continuity equation

$$\frac{\partial \psi}{\partial t} + \frac{\partial}{\partial M}(\psi \dot{M}) = 0, \quad (1)$$

where the dot denotes differentiation with respect to t . The formal solution of this equation is

$$\psi(M, t) = \psi_0(M_0) |\partial M_0 / \partial M|, \quad (2)$$

where $\psi_0(M) = \psi(M, 0)$ is the initial mass function, and $M_0(M, t)$ is the initial mass of a cluster that has a mass M at a later time t . In addition to these variables, the mass function may depend on the orbital parameters of the clusters, and hence their location within a galaxy, and may also vary from one galaxy to another. We first consider clusters on the same orbit. Later, we will average the mass function over realistic distributions of orbits and examine its dependence on the properties of the host galaxy.

We consider three processes that reduce the masses of star clusters: evaporation driven by two-body relaxation, evaporation driven by gravitational shocks, and mass loss driven by stellar evolution (supernovae, stellar winds, and other ejecta). Dynamical friction, combined with tidal limitation, also causes disruption, but this is only important near the centers of galaxies and is neglected here, mainly to simplify our analysis. More specifically, a cluster of mass M at a distance R from the center of a galaxy with a circular velocity V_c would be destroyed in a time $t_{df} \approx 60(V_c/220 \text{ km s}^{-1})(M/10^5 M_\odot)^{-1}(R/\text{kpc})^2 \text{ Gyr}$ (see equation 7-26 of Binney & Tremaine 1987). We have evaluated this expression for the 146 globular clusters in the Milky Way with known luminosities (assuming $M/L_V = 3$) and positions in the most recent compilation of data by Harris (1996, 1999). We find that only two clusters have $t_{df} < 10 \text{ Gyr}$ and only seven have $t_{df} < 20 \text{ Gyr}$; the vast majority have much larger t_{df} and are thus virtually immune to disruption by dynamical

friction. This suggests, but does not prove, that dynamical friction was also relatively unimportant in the past. Bulge shocks contribute to the disruption of clusters on highly elongated orbits, but they are probably less important than disk shocks for most clusters and are also neglected here. The rates of evaporation by bulge and disk shocks depend on the properties of the clusters and their orbits in similar ways. Thus, by including strong disk shocks near the centers of galaxies, we also mimic at least qualitatively the effects of bulge shocks.

As an approximation, we assume that the processes considered here—two-body relaxation, gravitational shocks, and stellar evolution—operate independently of each other, at fractional rates ν_{ev} , ν_{sh} , and ν_{se} . Thus, following many previous studies (see Spitzer 1987), we write

$$\dot{M} = -(\nu_{ev} + \nu_{sh} + \nu_{se})M, \quad (3)$$

with

$$\nu_{ev} = \frac{\xi_e}{t_{rh}} = \frac{7.25\xi_e m G^{1/2} \ln \Lambda}{M^{1/2} r_h^{3/2}}, \quad (4)$$

$$\nu_{sh} = \frac{7\kappa_s \bar{A}}{3t_{sh}} = \frac{15.6\kappa_s \bar{A} g_m^2 r_h^3}{G M P_\phi V_Z^2}. \quad (5)$$

In equation (4), ξ_e is the fraction of stars that escape per half-mass relaxation time t_{rh} by two-body scattering, r_h is the half-mass radius, m is the mean stellar mass, and $\ln \Lambda$ is the Coulomb logarithm. We neglect possible slow variations in the last two quantities and set $m = 0.7 M_\odot$ and $\ln \Lambda = 12$ in all our calculations. In equation (5), t_{sh} is the gravitational shock heating time for first-order energy changes in the impulse approximation (Ostriker, Spitzer, & Chevalier 1972) and \bar{A} is a correction for partial adiabatic (i.e., non-impulsive) response averaged over all the stars in a cluster (see Appendix A for details). The factor 7/3 accounts approximately for the addition of second-order energy changes, also known as shock-induced relaxation (Spitzer & Chevalier 1973; Kundić & Ostriker 1995). The other coefficient in equation (5) relates the fractional change in energy caused by gravitational shocks to the corresponding fractional change in mass, i.e., $\dot{M}/M = \kappa_s \dot{E}/E$. Also in equation (5), V_Z is the vertical component of the velocity of a cluster relative to the galactic disk, P_ϕ is the azimuthal period of its orbit around the galaxy, and $g_m = 2\pi G \Sigma_d$ is the maximum vertical acceleration caused by the disk of surface mass density Σ_d . We assume that the disk has an exponential profile all the way into the galactic center, $\Sigma_d(R) = \Sigma_d(0) \exp(-R/R_d)$, thus helping to mimic the effects of bulge shocks. The fractional rate of mass loss by stellar evolution depends on the age of a cluster and the stellar initial mass function (IMF). We compute $\nu_{se}(t)$ from the Leitherer et al. (1999) models with the Salpeter IMF.

We assume each cluster has an outer, limiting radius r_t determined by the tidal field of the host galaxy at the pericenter of its orbit. Clusters on orbits with fixed pericenters, such as those in a static, spherical galactic potential, as assumed here, will therefore evolve at constant mean density, $\bar{\rho} = M/(4\pi r_t^3/3)$; and clusters on orbits with different pericenters will have different $\bar{\rho}$ (with an additional weak dependence on the shape of the orbits, resulting from the centrifugal acceleration at pericenter; see equation (15) below). This is a standard assumption, although it is not expected

to be perfect except possibly for circular orbits (Spitzer 1987). The assumption that the clusters are tidally limited is justified by the fact that, if they initially extended beyond r_t , their outer parts would be stripped off after a few orbits, whereas if they did not initially extend to r_t , they would expand as a result of the disruptive effects considered here, predominantly stellar mass loss in the early stages, until they reached r_t . Some clusters with low central concentrations might be destroyed relatively quickly by a combination of stellar evolution and tidal limitation, with little or no help from two-body relaxation or gravitational shocks (Chernoff & Weinberg 1990; Fukushige & Heggie 1995); these clusters are not included in our calculations.

We must now specify the escape probability parameter for two-body relaxation ξ_e , the energy-mass conversion factor for gravitational shocks κ_s , and the relation between the half-mass and tidal radii, r_h and r_t . A valuable point of reference is Hénon’s (1961) model for the self-similar evolution of a tidally limited cluster with a single stellar mass by two-body relaxation alone. This has $\xi_e = 0.045$ and $r_h = 0.145r_t$. The Hénon model is often regarded as an adequate approximation for high-concentration clusters before core collapse, which typically occurs about half way through their lifetimes, and an excellent approximation for all clusters after core collapse. The value of ξ_e found in Monte Carlo and Fokker Planck models with a single stellar mass is typically 2–3 times below the Hénon value in the early stages of evolution and closer to it in the late stages (Spitzer & Chevalier 1973; Lee & Ostriker 1987; Gnedin, Lee, & Ostriker 1999). On the other hand, models with a realistic spectrum of stellar masses evolve a few times faster than those with a single stellar mass (Johnstone 1993; Lee & Goodman 1995). Thus, in most of our calculations, we adopt the Hénon value of ξ_e as a reasonable approximation to the effective escape probability parameter for the entire evolution of a realistic cluster, including both its pre- and post-core collapse phases. We also adopt the relation between r_h and r_t in the Hénon model.

The energy-mass conversion factor κ_s depends on how the energy imparted to a cluster by gravitational shocks is divided between bound and escaping stars. The detailed, but non-evolutionary calculations by Chernoff et al. (1986) give $\kappa_s \approx 1$ for high-concentration clusters (κ_s is $-\nu/f$ in their notation). In the evolving Monte Carlo models of Spitzer & Chevalier (1973), which include two-body relaxation and the first- and second-order energy changes caused by impulsive gravitational shocks, the total evaporation rate is given to an accuracy of about 30% by equation (3) with $\nu_{sh} = 2/t_{sh}$, corresponding to $\kappa_s \approx 1$ (see also Section 5-2b of Spitzer 1987). Recent Fokker-Planck calculations indicate that the rates of evaporation by two-body relaxation and gravitational shocks, ν_{ev} and ν_{sh} , are sometimes correlated and mutually reinforcing (Gnedin et al. 1999). The effect appears to be important mainly when the two rates are comparable. We neglect this complication and adopt $\kappa_s = 1$. This and our adopted value of ξ_e ensure that our simple model has the correct behavior when either two-body relaxation or gravitational shocks dominate, i.e., in the limits $\nu_{ev} \gg \nu_{sh}$ and $\nu_{ev} \ll \nu_{sh}$, and thus when the masses of clusters are either small or large (relative to M_p). As we show later, these limiting cases play a major role in determining the shape of the mass function of the clusters.

With the assumptions discussed above, equations (3)–(5) take the form

$$\dot{M} = -\mu_{ev} - (\nu_{sh} + \nu_{se})M, \quad (6)$$

where

$$\mu_{ev} = 269 \xi_e (G\bar{\rho})^{1/2} m \ln \Lambda, \quad (7)$$

$$\nu_{sh} = \frac{0.0113 \kappa_s \bar{A} g_m^2}{G\bar{\rho} P_\phi V_Z^2} \quad (8)$$

are constants and ν_{se} is a function of time. This has the exact solution

$$M = \{M_0 - \mu_{ev} \int_0^t \exp[\nu_{sh} t' + S(t')] dt'\} \exp[-\nu_{sh} t - S(t)], \quad (9)$$

with

$$S(t) = \int_0^t \nu_{se}(t') dt'. \quad (10)$$

Equation (9) can be inverted to obtain $M_0(M, t)$, and this can then be substituted into equation (2) to obtain $\psi(M, t)$ for any specified initial mass function $\psi_0(M)$.

Figure 1 shows the evolution of the mass M predicted by equations (7)–(10) for three clusters with different initial masses M_0 on the same orbit (with the parameters specified in the caption). In the early stages ($t \lesssim 3 \times 10^8$ yr), the mass drops approximately exponentially with time as a result of stellar evolution until it reaches about 60% of its initial value. Thereafter, the mass declines exponentially with time as a result of gravitational shocks and linearly with time as a result of two-body relaxation. Gravitational shocks become relatively less important with decreasing mass, and two-body relaxation always dominates in the late stages as the mass approaches zero. The evolution predicted by this simple analytical model is generally similar to that found in the more accurate Monte Carlo, Fokker-Planck, and N-body models, although there are differences in detail (see the references cited above in connection with the parameters ξ_e and κ_s). However, even the most sophisticated models still involve some important idealizations, and they sometimes differ from each other by as much as they differ from our simple model. These comparisons indicate that the approximate evolution specified by equations (7)–(10) is suitable for our purposes.

It is worth pausing here to consider separately the influence of each disruptive effect on the mass function. This is simplest for a set of clusters on the same galactic orbit (i.e., with the same values of μ_{ev} and ν_{sh}). Inserting equations (9) and (10) with $\nu_{sh} = \nu_{se} = 0$, $\mu_{ev} = \nu_{se} = 0$, and $\mu_{ev} = \nu_{sh} = 0$ into equation (2) gives

$$\psi(M, t) = \psi_0(M + \mu_{ev} t) \quad \text{two-body relaxation alone,} \quad (11)$$

$$\psi(M, t) = e^{\nu_{sh} t} \psi_0(M e^{\nu_{sh} t}) \quad \text{gravitational shocks alone,} \quad (12)$$

$$\psi(M, t) = e^{S(t)} \psi_0(M e^{S(t)}) \quad \text{stellar evolution alone.} \quad (13)$$

For two-body relaxation alone, the masses of clusters decrease linearly with time. This flattens the mass function at low masses but has little effect on its shape at high masses, i.e., $\psi(M, t) = \text{const}$

for $M \lesssim \mu_{ev}t$ and $\psi(M, t) = \psi_0(M)$ for $M \gtrsim \mu_{ev}t$. Thus, if the mass function is initially a power law, $\psi_0(M) \propto M^\beta$ with $\beta < 0$, it will develop a bend at $M \approx \mu_{ev}t$. In contrast, for gravitational shocks or stellar evolution alone, the masses of clusters decrease exponentially or approximately exponentially with time. This preserves the shape of the mass function in the sense that both ψ and M are simply rescaled by time-dependent factors. Thus, if the mass function is initially a power law, it will remain one at all later times: $\psi(M, t) \propto \psi_0(M) \propto M^\beta$. In the case of gravitational shocks, the rescaling factor increases indefinitely, whereas in the case of stellar evolution, it saturates at $\exp S(t) \approx 1.6$ for $t \gtrsim 3 \times 10^8$ yr. As we show later, the scaling relations derived here are approximately correct even when the mass function is averaged over realistic distributions of orbits (i.e., with different values of μ_{ev} and ν_{sh}).

We now consider clusters on different orbits within a galaxy. This is assumed for simplicity to have a static, spherically symmetric potential $\Phi(R)$, where R denotes the galactocentric radius in spherical (not cylindrical) polar coordinates. Thus, we can characterize each orbit by the constant values of the energy E and angular momentum J per unit mass and the angle θ between the normals of the orbital plane and the disk. For some purposes, it is useful to reexpress E and J in terms of the pericenter and apocenter of the orbit, R_p and R_a , and the radius R_c of a circular orbit with the same energy

$$E = \frac{1}{2}V_c^2(R_c) + \Phi(R_c) = \frac{1}{2}(J/R_{p,a})^2 + \Phi(R_{p,a}), \quad (14)$$

where V_c is the circular velocity. We further assume that the mass distribution of the galaxy can be modeled as a singular isothermal sphere, with $\Phi(R) = V_c^2 \ln R$ and $V_c = \text{const}$. In this case, the mean density of a cluster is given by

$$\bar{\rho}(E, J) = \frac{1}{\pi G} \left(\frac{3}{2}\right)^4 \left[1 - \ln\left(\frac{R_p}{R_c}\right)\right] \left(\frac{V_c}{R_p}\right)^2. \quad (15)$$

We note that this depends mainly on the pericenter of the orbit and only weakly (logarithmically) on the shape of the orbit. Equation (15) is based on the formula for the tidal radius advocated by Innanen, Harris, & Webbink (1983), which accounts approximately for the tidal elongation of clusters. The mean density would be reduced by the factor $(2/3)^3$ if the King (1962) formula for r_t were adopted. The precise form of $\bar{\rho}$ is still an open issue in the case of non-circular orbits, but it is likely that equation (15) captures the primary dependence on E and J , which is sufficient for our purpose.⁴ Inserting $\bar{\rho}(E, J)$ into equation (7) gives the rate of evaporation by two-body relaxation μ_{ev} as a function of E and J .

To compute the fractional rate of evaporation by gravitational shocks ν_{sh} as a function of E and J , we average the corresponding rate over R and θ , weighting by the number of clusters with each of these coordinates. The number of clusters at any radius is proportional to the time

⁴The best observational evidence that equation (15) is at least approximately correct is the strong inverse correlation between the mean densities of globular clusters in the Milky Way and their present galactocentric distances, $\bar{\rho} \propto R^{-1.7 \pm 0.2}$ (see Fig. 7 of Innanen et al. 1983). For many position-velocity distributions, this implies a similar, if not identical, relation between $\bar{\rho}$ and R_p .

spent there and hence inversely proportional to the radial component of the velocity there. The orientations of the orbits are assumed to be random. Thus, we have

$$\bar{\nu}_{sh}(E, J) = \frac{2}{P_R} \int_{R_p}^{R_a} \frac{dR}{V_R(R)} \int_0^{\pi/2} \nu_{sh}(E, J, R, \theta) \sin \theta d\theta. \quad (16)$$

Here, the functional dependence of ν_{sh} on E , J , R , and θ follows from equation (8) and the adiabatic correction factor \bar{A} (see Appendix A and Figure 12). The radial and azimuthal periods of the orbits are given by

$$P_R = 2 \int_{R_p}^{R_a} \frac{dR}{V_R(R)}, \quad (17)$$

$$\frac{1}{P_\phi} = \frac{J}{\pi P_R} \int_{R_p}^{R_a} \frac{dR}{R^2 V_R(R)}. \quad (18)$$

Furthermore, the radial and vertical components of the velocity (relative to the disk) are given by

$$V_R = [2E - (J/R)^2 - 2\Phi(R)]^{1/2}, \quad (19)$$

$$V_Z = V_T \sin \theta = (J/R) \sin \theta, \quad (20)$$

where V_T is the transverse component of the velocity (orthogonal to the radius in the orbital plane). Equation (20) is valid because, just as a cluster passes through the disk, the radial and vertical components of its velocity are orthogonal. This simplifies our calculations substantially. Inserting equations (8) and (20) into equation (16), we have

$$\bar{\nu}_{sh}(E, J) = \frac{0.0226\kappa_s}{G\bar{\rho}P_R P_\phi J^2} \int_{R_p}^{R_a} \frac{R^2 g_m^2(R)}{V_R(R)} dR \int_0^{\pi/2} \frac{\bar{A}(E, J, R, \theta)}{\sin \theta} d\theta. \quad (21)$$

When $\mu_{ev}(E, J)$ and $\bar{\nu}_{sh}(E, J)$ are substituted into equations (9), (10) and (2), we obtain the mass function $\psi(M, t; E, J)$ of clusters on orbits specified by E and J .

For some purposes, we are interested in how the mass function depends on position \mathbf{R} and velocity \mathbf{V} rather than energy E and angular momentum J . With this in mind, we define $f(M, \mathbf{R}, \mathbf{V}, t) dM d\mathbf{R} d\mathbf{V}$ as the number of clusters in the small element of mass-position-velocity space $dM d\mathbf{R} d\mathbf{V}$ centered on $(M, \mathbf{R}, \mathbf{V})$ at time t . We assume for simplicity that the cluster system is spherical and non-rotating.⁵ Thus, by the Jeans theorem, we have

$$f(M, \mathbf{R}, \mathbf{V}, t) = \psi(M, t; E, J) f_0(E, J), \quad (22)$$

⁵In fact, the cluster system would develop some asphericity, even if it initially had none, as a consequence of the different rates at which clusters with different orbital orientations are disrupted by disk shocks. The globular cluster systems in many galaxies consist of both a nearly spherical, slowly rotating (halo) component and a moderately flattened, rapidly rotating (disk) component. In the Milky Way, about 27% of the known globular clusters are members of the disk component [this is the fraction of clusters in the Harris (1996, 1999) compilation with metallicities above the disk-halo division $[\text{Fe}/\text{H}] = -0.8$ specified by Zinn (1985)]. A complete analysis of the disruption of clusters would take these complications into account. Our simple model should provide a good approximation to the mass function and its dependence on galactocentric radius, the main goals of this study, because we average the rate of evaporation by disk shocks over orbital orientations [see equations (16)–(21)] and because, for most clusters, disk shocks are not the dominant disruptive process.

where $f_0(E, J)$ is the initial distribution function, defined such that $f_0(E, J)d\mathbf{R}d\mathbf{V}$ is the fraction of clusters in the small element of position-velocity space $d\mathbf{R}d\mathbf{V}$ with energies and angular momenta near E and J at $t = 0$. Equation (22) implies that the disruption of clusters does not alter their orbits. The mass function at the radius $R = |\mathbf{R}|$ is given by the integral of $f(M, \mathbf{R}, \mathbf{V}, t)$ over all velocities; using equation (22) and evaluating the Jacobean for the transformation between (V_R, V_T) and (E, J) , we obtain

$$\begin{aligned}\psi(M, R, t) &= 4\pi \int_0^\infty dV_R \int_0^\infty V_T f(M, \mathbf{R}, \mathbf{V}, t) dV_T \\ &= \frac{4\pi}{R^2} \int_{\Phi(R)}^\infty dE \int_0^{J_m(E, R)} \frac{J\psi(M, t; E, J)f_0(E, J)}{[2E - (J/R)^2 - 2\Phi(R)]^{1/2}} dJ,\end{aligned}\quad (23)$$

where $J_m(E, R) = R[2E - 2\Phi(R)]^{1/2}$ is the maximum angular momentum of an orbit with a given energy E and radius R . Finally, we note that the average mass function in a volume bounded by radii R_1 and R_2 is

$$\bar{\psi}(M, t) = \frac{3}{R_2^3 - R_1^3} \int_{R_1}^{R_2} \psi(M, R, t) R^2 dR. \quad (24)$$

In the following, we consider two simple models for the initial distribution function of the clusters. The first is the Eddington model:

$$f_0(E, J) \propto \exp(-E/\sigma^2) \exp[-\frac{1}{2}(J/R_A\sigma)^2]. \quad (25)$$

This has velocity dispersions $\sigma_R = \sigma$ and $\sigma_T = \sigma[1 + (R/R_A)^2]^{-1/2}$ in the radial and transverse (i.e., orthogonal) directions, respectively, where the anisotropy radius R_A marks the transition from a nearly isotropic to a predominantly radial velocity distribution. In a logarithmic potential, the initial density profile (number of clusters per unit volume) is

$$n_0(R) \propto [1 + (R/R_A)^2]^{-1} R^{-\gamma} \quad (26)$$

with $\gamma = (V_c/\sigma)^2$. Distribution functions like the Eddington arise frequently in simulations of gravitational collapse, in which violent relaxation is nearly complete in the inner regions but not in the outer regions. The second model we consider has an initial distribution function of the form

$$f_0(E, J) \propto \exp(-E/\sigma^2) J^{-2\beta}. \quad (27)$$

In this case, the radial and transverse velocity dispersions are $\sigma_R = \sigma$ and $\sigma_T = \sigma(1 - \beta)^{1/2}$, and in a logarithmic potential, the initial density profile is a power law,

$$n_0(R) \propto R^{-2\beta - \gamma}, \quad (28)$$

again with $\gamma = (V_c/\sigma)^2$. We refer to this as the scale-free model. It is not clear which physical processes would produce a scale-free distribution function, although gravitational clustering in a self-similar hierarchy might do so. For our purposes, the most important difference between the

Eddington and scale-free models is that, in the former, the velocity anisotropy increases outward, whereas in the latter, it is the same at all radii. Thus, the distribution of pericenters is narrower in the Eddington model than it is in the scale-free model (see the formulae in Appendix B and Figure 13).

Before presenting the results of our calculations, we pause here to enumerate the parameters in our models. These are: the escape probability parameter ξ_e , the circular velocity of the galaxy V_c , the central surface density and scale radius of the disk, $\Sigma_d(0)$ and R_d , the index characterizing the initial density profile γ , and the anisotropy radius R_A (for the Eddington model) or the anisotropy parameter β (for the scale-free model). As standard values of these parameters, we adopt $\xi_e = 0.045$, $V_c = 220 \text{ km s}^{-1}$, $\Sigma_d(0) = 720 M_\odot \text{ pc}^{-2}$, $R_d = 3 \text{ kpc}$, and $\gamma = 2.5$, $R_A = 5 \text{ kpc}$ (Eddington) or $\gamma = 3.5$, $\beta = 0.5$ (scale-free). The first of these is the escape probability parameter in the Hénon (1961) model, which should approximate the effective value of ξ_e for the pre- and post-core collapse evolution of clusters with a realistic spectrum of stellar masses.

Our standard values of V_c , $\Sigma_d(0)$, and R_d are appropriate for the disk of the Milky Way (see Binney & Merrifield 1998). For example, the standard values of $\Sigma_d(0)$ and R_d imply that the surface density of the disk is $50 M_\odot \text{ pc}^{-2}$ at the solar position, $R = 8 \text{ kpc}$. Our standard values of γ were chosen so that the final density profile of the cluster system in the models would approximate the observed profile (see below). We have chosen the standard value of R_A to be the same as the median galactocentric radius of the globular clusters in the Milky Way, $R_h \approx 5 \text{ kpc}$. This ensures that the velocity anisotropy at R_h in the Eddington model is the same as that at all radii in the scale-free model, namely $\sigma_R = \sqrt{2}\sigma_T$. This is more radial anisotropy than appears to exist in the present velocity distribution of globular clusters in the Milky Way (Frenk & White 1980; Dinescu, Girard, & van Altena 1999). However, it is similar to the radial anisotropy of halo stars in the solar neighborhood (Binney & Merrifield 1998) and may be appropriate for the initial anisotropy of globular clusters (since clusters on elongated orbits are preferentially disrupted).

In the following, we explore the influence of different physical processes on the mass function by varying the parameters with respect to their standard values and comparing results from the Eddington and scale-free models. We calculate the mass function at times up to $t = 12 \text{ Gyr}$, the age of globular clusters in the Milky Way favored in several recent studies (Gratton et al. 1997; Reid 1997; Chaboyer et al. 1998).

3. Results

The aim of this section is to present the results of our calculations and to compare them with observations. Figure 2 shows the mass functions of young star clusters in the merging Antennae galaxies and old globular clusters in the Milky Way. The former is based on deep *UBVI* images taken with the WFPC2 on *HST* and mass-to-light ratios derived from stellar population synthesis models (Zhang & Fall 1999). The latter is based on the luminosities of the 146 clusters with

known distances in the most recent compilation of data by Harris (1996, 1999) and $M/L_V = 3$. Both samples are believed to be reasonably complete over the ranges plotted [$\log(M/M_\odot) > 3.8$ and $\log(M/M_\odot) > 2.9$, respectively]. If there is any incompleteness, however, it is likely that more clusters are missing from the low-mass ends of the functions. Here, and throughout this section, we have plotted the function $\Psi(\log M)$, the number of clusters per unit $\log M$, against $\log(M/M_\odot)$. This is related to the function $\psi(M)$ defined earlier, the number of clusters per unit M , by $\Psi(\log M) = (\log e)^{-1} M \psi(M)$. The use of $\Psi(\log M)$ facilitates some comparisons with observations. The dashed parabola in Figure 2 depicts the usual lognormal mass function with a peak at $M_p = 2 \times 10^5 M_\odot$ and a dispersion of $\sigma(\log M) = 0.5$, corresponding to a Gaussian distribution of magnitudes with $\langle M_V \rangle = -7.3$ and $\sigma(M_V) = 1.2$ (for $M/L_V = 3$).

As we have already mentioned, and as Figure 2 also demonstrates, the shapes of the mass functions of the young clusters in the Antennae and the old clusters in the Milky Way are very different. The former declines monotonically as $\Psi(\log M) \propto M^{-1}$, whereas the latter rises to a peak at $M_p \approx 2 \times 10^5 M_\odot$ and then declines. Another fact evident from Figure 2 is that the lognormal function provides a good representation of the empirical mass function (histogram) of globular clusters at high masses but not at low masses. For $M \lesssim M_p$, the observations can be fitted better by $\Psi(\log M) \propto M$, corresponding to $\psi(M) = \text{const}$. This behavior in the empirical mass function was first shown by McLaughlin (1994). As we have pointed out here—for the first time we believe—the form $\psi(M) = \text{const}$ is a robust signature of evaporation by two-body relaxation. This behavior in the mass function can be traced to the fact that, in the late stages of evolution, the masses of tidally limited clusters decrease linearly with time. Thus, the time dt they spend in each small interval of mass $dM = \dot{M}dt$ is independent of M , leading to $\psi(M) = \text{const}$.⁶

The results of our calculations are presented in Figures 3–11. In these diagrams, we plot the mass function at times $t = 0, 1.5, 3, 6$, and 12 Gyr. The peak of $\Psi(\log M)$ at $t = 12$ Gyr is indicated by an upward-pointing arrow. We first explore the effects of different initial mass functions with the parameters fixed at their standard values. Figure 3 shows the evolution of the mass functions, averaged over all radii (actually, $1 < R < 100$ kpc) for the Eddington initial distribution function; Figure 4 shows the corresponding results for the scale-free initial distribution function. The four initial mass functions we consider are: (1) a power law, $\psi_0(M) \propto M^\beta$ with $\beta = -2$, (2) the same power law but truncated below $M = 3 \times 10^5 M_\odot$, (3) a Schechter function, $\psi_0(M) \propto M^\beta \exp(-M/M_*)$ with $\beta = -2$ and $M_* = 5 \times 10^6 M_\odot$, (4) a lognormal function, $\psi_0(M) \propto \exp\{-\frac{1}{2}[\log(M/M_p)/\sigma(\log M)]^2\}$ with $M_p = 2 \times 10^5 M_\odot$ and $\sigma(\log M) = 0.5$.

In all our models, the mass function develops a peak, and at $t = 12$ Gyr, this is remarkably close to the observed peak, despite the very different initial conditions. For low-mass clusters ($M \lesssim M_p$), the disruption is dominated by two-body relaxation, which, as noted above, leads to $\psi(M) = \text{const}$ and $\Psi(\log M) \propto M$, in excellent agreement with the empirical mass function (histograms). This is true whether the initial mass function lies above or below the relation $\psi(M) = \text{const}$, as illustrated

⁶This is consistent with the relation $dN/dt_{rh} = \text{const}$ at small t_{rh} noted by Hut & Djorgovski (1992).

in the left- and right-hand panels of Figures 3 and 4. Even if the formation of low-mass clusters were suppressed entirely, they would appear later as the remnants of intermediate-mass clusters on their way to destruction. High-mass clusters ($M \gtrsim M_p$) are mainly affected by stellar evolution and gravitational shocks. For the reasons given above, these shift $\Psi(\log M)$ to smaller $\log M$ but leave its shape nearly invariant (when dynamical friction is neglected). Thus, the empirical mass function can always be matched above the peak by a suitable choice of the initial mass function, as illustrated in the lower panels of Figures 3 and 4, with the Schechter and lognormal functions. Unfortunately, neither theory nor observation provides much guidance on the form of $\psi_0(M)$ at high M . Because of small-number statistics, the mass function of old globular clusters in the Milky Way is uncertain above $10^6 M_\odot$, and that of young star clusters in the Antennae above $3 \times 10^5 M_\odot$ (see Figure 2).

We have also computed the total number of clusters $N_T(t)$ and their total mass $M_T(t)$ by integrating $\psi(M, t)$ and $M\psi(M, t)$ over M . Table 1 lists the present disruption rates, $|\dot{N}_T/N_T|$ and $|\dot{M}_T/M_T|$, and the present survival fractions, N_T/N_{T0} and M_T/M_{T0} , for the four different initial conditions shown in Figure 3. In the two cases with steep initial mass functions, the survival fractions depend on the lower cutoff M_l of the integration over M ; thus, we list results for a range of values, $M_l = 1 - 10^4 M_\odot$. The other entries in Table 1 are not sensitive to M_l . We note that the timescales for the disruption of existing clusters, $|\dot{N}_T/N_T|^{-1}$ and $|\dot{M}_T/M_T|^{-1}$, are comparable to the present age (actually 1 – 4 times longer). The reason for this is that most of the clusters with shorter disruption timescales have already perished. The present values of $|\dot{N}_T/N_T|$ in our models agree with the total disruption rate of globular clusters in the Milky Way estimated by Hut & Djorgovski (1992) from the empirical distribution of half-mass relaxation times ($\dot{N}_T = -5 \pm 3 \text{ Gyr}^{-1}$ and $N_T = 98$). Furthermore, the present values of $|\dot{M}_T/M_T|$ are similar to the typical (median) disruption rates of individual globular clusters estimated by Gnedin & Ostriker (1997). We find that the present total number and mass of clusters, N_T and M_T , are small fractions of their initial values, N_{T0} and M_{T0} , especially when the initial mass function rises toward low masses. The values of M_T/M_{T0} , in particular, indicate that a substantial fraction of the field stars in the galactic spheroid could be the debris of disrupted clusters. However, even in the most extreme case considered here (the Schechter initial mass function with a lower cutoff at $M_l = 1 M_\odot$), the survival fraction is a few times larger than the ratio of the mass in globular clusters to the mass in the galactic spheroid (about 1%). Thus, to account for all the field stars in the spheroid by disrupted clusters, the initial mass function would have to rise more steeply than $\psi_0(M) \propto M^{-2}$ for $M \lesssim 10^4 M_\odot$.

In Figure 5, we plot the number density profiles of the cluster system at different times for the Eddington and scale-free initial distribution functions and the Schechter initial mass function. The profiles become flatter because clusters are destroyed faster near the galactic center, although a nearly steady form is reached by $t \approx 1.5 \text{ Gyr}$. The final profiles in both models are in reasonable, although not perfect, agreement with the observed profile, which we have derived from the same compilation of data as we used for the mass function (Harris 1996, 1999). In fact, we chose the standard values of the parameter $\gamma = (V_c/\sigma)^2$, after some adjustment, to achieve this match.

Figures 6 and 7 show the evolution of the mass function for the same models when averaged over the inner and outer parts of the galaxy ($R < 5$ kpc and $R > 5$ kpc), the boundary between these being close to the median radius of globular clusters in the Milky Way. In both cases, the peak mass is higher in the inner region. This is caused by the higher rate of two-body relaxation, resulting from the higher mean density, and the higher rate of gravitational shocks near the galactic center, the former effect being more important than the latter (see below). For the Eddington model, the logarithmic difference in the peak mass between inner and outer clusters is $\Delta \log M_p = 0.2$, corresponding to a difference in mean absolute magnitudes of $\Delta \langle M_V \rangle = 0.5$ (for constant M/L_V). For the scale-free model, the differences are $\Delta \log M_p = 0.65$ and $\Delta \langle M_V \rangle = 1.6$. For comparison, we find $\Delta \langle M_V \rangle = 0.16 \pm 0.26$ for the globular clusters with $R < 5$ kpc and $R > 5$ kpc in the Harris (1996, 1999) compilation. Thus, the radial variation of the peak mass in the Eddington model is consistent with observations (at the 1.3σ level), whereas that in the scale-free model is not. Furthermore, the width of the mass function in the Eddington model agrees better with the observed one. The explanation for these differences in the mass functions can be found in the different radial variations of the velocity anisotropy in the two models. In the Eddington model, the anisotropy increases outward, causing a relatively narrow distribution of pericenters and hence disruption rates; in the scale-free model, the anisotropy is constant, causing a relatively wide distribution of pericenters and disruption rates (see Appendix B). From now on, we consider only models with the Eddington initial distribution function.

The effect of changing the escape probability parameter ξ_e is shown in Figure 8. As expected, the evolution of the mass function is slower and the peak mass is smaller for smaller ξ_e and conversely for larger ξ_e . The effective value of ξ_e is not known precisely, although we have argued above that it should be close to the Hénon and our standard value (0.045) when allowance is made for both the pre- and post-core collapse evolution of clusters with a realistic spectrum of stellar masses. In fact, the similarity between the peak mass in our models and the observations indicates that the actual value of ξ_e cannot differ from our standard value by more than a factor of about two.

In Figure 9, we show the effects of varying the velocity anisotropy radius R_A on the mass function of clusters in the inner and outer parts of the galaxy ($R < 5$ kpc and $R > 5$ kpc). Small values of R_A imply predominantly radial orbits, with mostly small pericenters and hence large mean densities, whereas large values of R_A imply a nearly isotropic velocity distribution, with a wide range of pericenters and mean densities. This is why the mass function evolves faster and the peak mass is larger for smaller R_A . Moreover, the more radial are the orbits, the more similar are the peak masses in the inner and outer parts of the galaxy. For $R_A = 2.5$ kpc, we find $\Delta \log M_p \approx 0$, whereas for $R_A = 15$ kpc, we find $\Delta \log M_p = 0.5$. These correspond, respectively, to $\Delta \langle M_V \rangle \approx 0$ and 1.2 (for constant M/L_V). The former is consistent with the observed value, $\Delta \langle M_V \rangle = 0.16 \pm 0.26$, whereas the latter is probably not. Thus, a substantial degree of radial anisotropy is required in the initial velocity distribution for consistency with the weak radial variation in the empirical mass function. The present velocity distribution may in fact be nearly isotropic (Frenk & White 1980), but as a result of the preferential disruption of clusters on elongated orbits, the initial distribution

would have been more anisotropic.

Figure 10 shows the effects of altering the surface density of the disk. Here, we present results for an exponential disk with double the standard central density, i.e., $\Sigma_d(0) = 1440 M_\odot \text{pc}^{-2}$, and for no disk at all. Figure 10 also indicates how our results depend on the energy-mass conversion factor κ_s since the rate of evaporation by gravitational shocks is proportional to $\kappa_s \Sigma_d^2$. As expected, a more massive disk causes the mass function of star clusters to evolve faster. However, in this case, unlike two-body relaxation, the peak mass decreases. The reason for this is that, as noted above, gravitational shocks shift the mass function to smaller masses while leaving its shape nearly invariant. However, gravitational shocks are less important than two-body relaxation in the disruption of low-mass clusters, even allowing for possible uncertainties in κ_s and Σ_d . This conclusion is also supported by the N-body models of Vesperini & Heggie (1997). Thus, the peak mass and its radial variation and the low-mass shape of the mass function are all determined primarily by two-body relaxation rather than gravitational shocks, contrary to some statements in the literature.

All our previous results were computed for a galaxy like the Milky Way, with $V_c = 220 \text{ km s}^{-1}$. It is also of interest to know how the mass function would evolve in other galaxies, with different circular velocities. For this purpose, we assume that the masses and sizes of galaxies scale as $M_g \propto V_c^k$ and $R_g \propto V_c^{k-2}$ (to satisfy the virial theorem, $V_c^2 \propto M_g/R_g$). Then the mean internal densities of star clusters, like those of their host galaxies, scale as $\bar{\rho} \propto M_g/R_g^3 \propto V_c^{6-2k}$. Recent estimates of the exponent in the baryonic Tully-Fisher relation lie in the range $k \approx 3-4$ (Bell & de Jong 2001, and references therein). For k at the lower end of the range, the mass function of star clusters is independent of V_c (since $\bar{\rho}$ is independent of V_c). For k at the upper end of the range, the mass function has the dependence on V_c shown in Figure 11. In this case, the peak mass decreases by $\Delta \log M_p = 0.5$ ($\Delta \langle M_V \rangle = 1.2$) as V_c increases from 110 to 440 km s^{-1} . This is probably larger than allowed by observations (Harris 1991). More definitive comparisons will require better knowledge of the relations between M_g , R_g , and V_c and possibly more complicated models for the internal structure of galaxies (e.g., with finite core radii). Moreover, dynamical friction, which is neglected in our models, may be important in galaxies with small V_c .

4. Comparison With Previous Studies

Several other researchers have suggested that disruptive processes would cause the mass function of star clusters to evolve toward something like a lognormal function. Okazaki & Tosa (1995) based their analysis on the survival triangle in the mass-radius (i.e., $\log M$ - $\log r_h$) plane, defined by setting the characteristic timescales for evaporation by two-body relaxation and gravitational shocks, t_{ev} and t_{sh} , equal to the current time t (Fall & Rees 1977). Okazaki & Tosa assumed that clusters inside the triangle would exist without any loss of mass ($M = M_0$ for $t_{ev} > t$ and $t_{sh} > t$), while clusters outside the triangle would not exist at all ($M = 0$ for $t_{ev} < t$ or $t_{sh} < t$). In other words, the mass of each cluster was assumed to be a step function of time, with the step at $t = \min(t_{ev}, t_{sh})$, rather than to decrease continuously with time as shown in Figure 1. The clusters

were postulated to have a power-law initial mass function and a Gaussian initial distribution of $\mu \equiv \log(M/r_h^\beta)$, with $\beta = 2.6$ or 4.1 . The mass function at later times was then obtained from this by integrating over r_h with the limits of integration set by the survival triangle. In this approach, the shape of the present mass function is determined largely by the assumed shape of the initial distribution of μ , which is not explained. Ostriker & Gnedin (1997) followed the same approach in a study of the radial variation of the mass function, except that they postulated a bivariate Gaussian initial distribution of $x \equiv \log(M/r_h^3)$ and $y \equiv \log M$ and integrated over the survival triangle in these coordinates, including the side for dynamical friction.

The evolution of the mass function of star clusters by disruptive processes was also considered by Elmegreen & Efremov (1997). They claimed this evolution would take the form $\psi(M, t) = \psi_0(M) \exp[-\nu(M)t]$ with $\nu(M) = \dot{M}/M$. Unfortunately, this is not correct, as one may verify by direct substitution into equation (1). Elmegreen & Efremov also claimed the disruption rate would have a strong inverse dependence on mass, $\nu \propto M^{-\gamma}$ with $\gamma \approx 2$. This is based on the current disruption rates of surviving clusters estimated by Gnedin & Ostriker (1997). However, since the correlation between ν and M is relatively weak, the value of γ estimated in this way is quite uncertain (see Figure 2 of Elmegreen & Efremov 1997). In fact, the data appear to be equally consistent with $\nu \propto M^{-1}$, the relation expected for the disruption of tidally limited clusters by two-body relaxation [see equations (6) and (7) here]. The mass function proposed by Elmegreen & Efremov has a peak at a few $\times 10^5 M_\odot$ and approaches the initial mass function for higher masses, but its shape for lower masses, where disruption is important, differs markedly from the solutions presented here.

Murali & Weinberg (1997a,b,c) studied the disruption of star clusters by two-body relaxation and gravitational shocks using a series of Fokker-Planck models. They followed the evolution of cluster systems with a halo component alone and with both halo and disk components. The initial distribution functions of the halo and disk components were represented by the scale-free model (called the Mestel sphere) and the Mestel disk, respectively, while the initial mass function was represented by a truncated power law. Murali & Weinberg (1997c) found that this model, with suitable choices of parameters, could reproduce many of the observed properties of the globular cluster system in the Milky Way. However, with the Fokker-Planck approach, they could only follow the evolution of clusters on a relatively sparse grid ($5 \times 4 \times 5$) in the variables R_a , M , and J/J_c . The four mass bins covered the range $1 \times 10^5 < M < 5 \times 10^6 M_\odot$, thereby excluding the low-mass clusters most susceptible to disruption. In any case, since Murali & Weinberg did not display the mass function at later times, we cannot make useful comparisons between our results and theirs.

Vesperini (1997, 1998) used analytical and semi-analytical models to study the evolution of the mass function of star clusters resulting from two-body relaxation, gravitational shocks, stellar evolution, and dynamical friction. He assumed the clusters were tidally limited and on circular orbits perpendicular to the galactic disk. The initial mass function was assumed to be a truncated power law or a lognormal function. Vesperini found in many cases that the final mass function

in his models resembled the empirical mass function of old globular clusters. However, for the truncated power law, the peak of the final mass function was well below the observed peak unless the truncation mass was large, i.e., $M_l \gtrsim 10^5 M_\odot$. In addition, the mass functions in Vesperini's models have a strong dependence on galactocentric radius because, with all the clusters on circular orbits, no radial mixing occurs. As we have shown here, the low-mass end of the empirical mass function of globular clusters can be reproduced even if the initial mass function has no truncation (i.e., with $M_l = 0$). Moreover, we find that radial mixing of orbits is necessary to account for the weak radial dependence of the empirical mass function. Vesperini speculated that the lognormal mass function represented a quasi-equilibrium distribution. We find instead that the high-mass shape of the mass function, whatever its initial form, is approximately preserved, while the low-mass shape, $\psi(M) = \text{const}$, is flatter than the lognormal function. Vesperini (2000, 2001) has recently used his models to predict the radial variation and dependence of the mass function of star clusters on the properties of their host galaxies (although the clusters are still assumed to be on circular orbits).

Baumgardt (1998) studied the evolution of the mass function of star clusters resulting from two-body relaxation and dynamical friction but not gravitational shocks or stellar evolution. He assumed the clusters were tidally limited at the pericenters of their orbits and approximated their disruption by means of a simple analytical model. Baumgardt computed the orbits of the clusters numerically, with energies and angular momenta drawn from an initial distribution function similar, but not identical, to our scale-free model (note that γ in his notation is $\gamma + 2\beta$ in our notation). He adopted a power-law initial mass function with $\beta = -2$ and a broad initial distribution of half-mass radii. Baumgardt found that the mass function developed a peak and that, after a Hubble time, this coincided roughly with the peak in the empirical mass function of old globular clusters. He also found that the peak mass was larger at smaller radii, with $\Delta \log M_p \approx 0.4$ ($\Delta \langle M_V \rangle \approx 1.0$) for clusters inside and outside $R = 10$ kpc, and he noted that this was probably incompatible with observations. Our results for the scale-free model generally agree with Baumgardt's, although detailed comparisons are difficult because his mass functions are very noisy. As we have shown here, the mass function in the Eddington model has a weaker radial variation than that in the scale-free model, in satisfactory agreement with observations.

5. Discussion

We have presented a series of simple, largely analytical models to compute the effects of disruption on the mass function of star clusters. Our models include evaporation by two-body relaxation and gravitational shocks and mass loss by stellar evolution. A virtue of our approach is that it leads to a clear understanding of how each disruptive process shapes the mass function of star clusters. Our goal has been to determine under what initial conditions the mass function evolves into a form resembling that of old globular clusters. We make two idealizations to simplify our calculations. First, we neglect correlations between the effects of two-body relaxation and

gravitational shocks. A comparison with more accurate Monte Carlo, Fokker-Planck, and N-body models indicates that the errors introduced by this approximation are acceptably small, especially for low- and high-mass clusters. Second, we assume the galactic potentials in which the clusters move are static and spherical. This ensures that the pericenter of each orbit remains fixed. We discuss below how our results would be modified if the galactic potentials were time-dependent and/or non-spherical.

We find that, for a wide variety of initial conditions, the mass function in our models develops a turnover or peak, which, after 12 Gyr, is remarkably close to the observed peak in the mass function of globular clusters ($M_p \approx 2 \times 10^5 M_\odot$). Below the peak, the evolution is dominated by two-body relaxation, and the mass function always develops a tail of the form $\psi(M) = \text{const}$. This reflects the linear decrease in the masses of tidally limited clusters with time just before they are destroyed. The predicted form of $\psi(M)$ at and below the peak coincides well with the observed form. We interpret this as strong support for the idea that evaporation by two-body relaxation played a major role in shaping the mass function of globular clusters at low and intermediate masses ($M \lesssim M_p$). Above the peak, the evolution of the mass function is dominated by stellar evolution at early times and by gravitational shocks at late times (when dynamical friction is neglected). These processes operate at fractional rates that are independent of the masses of the clusters and hence tend to preserve the shape of the mass function at high masses (in a log-log plot). We also find that the disruption of clusters can contribute substantially to the field star population in the galactic spheroid if the initial mass function of the clusters rises steeply toward low masses.

The radial variation of the mass function within a galaxy depends on the initial position-velocity distribution of the clusters. The reason for this is that the rate of evaporation by two-body relaxation and gravitational shocks depends on the orbits of the clusters, especially their pericenters. If most of the orbits are circular or if the velocity distribution is isotropic, the mass function will vary more with galactocentric radius than is observed. This variation can be reduced by the greater radial mixing that occurs when the velocity distribution has some radial anisotropy. However, to obtain a nearly uniform mass function within a galaxy, the radial anisotropy must increase outward, producing a distribution of pericenters that is narrower than the distribution of instantaneous positions of the clusters. We illustrate this by our models with Eddington and scale-free initial distribution functions, both of which have the same anisotropy at the median radius of the globular cluster system. In the former, the radial variation of the mass function is compatible with observations, whereas in the latter, it is not. Unfortunately, the initial position-velocity distribution of globular clusters is not known because most of the original clusters have been destroyed. However, since the destruction occurs preferentially for clusters on elongated orbits, the initial velocity distribution must have been more anisotropic than the present one.

Our conclusions to this point are based on models with static, spherical galactic potentials. In such models, each cluster returns to the same pericenter on each revolution about the galaxy. In galaxies with non-spherical potentials, however, the pericenter of a cluster may change from one revolution to the next. This effect should help to dilute the radial variation of the mass function.

An even more effective mixing of pericenters and consequent homogenization of the mass function may occur in galaxies with time-dependent potentials. Large variations in the potential are a natural consequence of the formation and evolution of galaxies by hierarchical clustering. Each time one galaxy merges with another, the orbits of the clusters are likely to be scrambled to some degree by violent relaxation. In this way, the mass functions of clusters in the inner and outer parts of the galaxies would also be combined or averaged, erasing any prior radial variations. In the hierarchical picture, merging is expected to be important early in the histories of all galaxies and late in the histories of some galaxies. It is not clear, however, whether merging occurred recently enough in most galaxies to account for the observed uniformity of the mass functions of their globular clusters. It is doubtful, for example, that the Milky Way or Andromeda galaxies experienced any major mergers in the last 8 Gyr or so (otherwise, their old disks would have been disrupted). Nevertheless, the mass functions of globular clusters in galaxies with time-dependent and/or non-spherical potentials should have less radial variation than those in the idealized models presented here.

Our models and some of those mentioned in the previous section have several observational implications. The first is that the peak of the mass function of clusters should increase with age. This might be observable in galaxies in which clusters formed continuously over long periods of time. Alternatively, the evolution of the peak mass might be observable in galaxies with bursts of cluster formation at different times, such as in a sequence of merger remnants. This test may be difficult, however, because the luminosity corresponding to the peak mass is relatively small for young clusters (since M_p varies more rapidly with t than M/L_V does). The second observational implication is that the peak mass should decrease with increasing distance from the centers of galaxies, unless this has been completely diluted by the mixing of pericenters discussed above. Searches for radial variations in the peak mass have so far been inconclusive. This test is difficult because the diffuse light of the galaxies also varies with radius, making it harder to find faint clusters in the inner regions. Finally, the strong dependence of the peak mass on the ages of clusters and the weak dependence on their positions within and among galaxies cast some doubt on the use of the peak luminosity as a standard candle for distance estimates. This method may be viable, however, if the samples of clusters are carefully chosen from similar locations in similar galaxies.

Our models also have implications for attempts to understand the formation of star clusters of different types. The shape of the mass function above the peak is largely preserved as clusters are disrupted and hence should reflect processes at the time they formed. Below the peak, however, the shape of the mass function is determined entirely by disruption, mainly driven by two-body relaxation, and hence contains no information about how the clusters formed. If there were any feature in the initial mass function, such as a Jeans-type lower cutoff, it would have been erased. In our models, the only feature in the present mass function, the peak at $2 \times 10^5 M_\odot$, is largely determined by the condition that clusters of this mass have a timescale for disruption comparable to the Hubble time. Thus, it is conceivable that star clusters of different types (open, populous, globular, etc) formed by the same physical processes with the same initial mass function and that the

differences in their present mass functions reflect only their different ages and local environments, primarily the strength of the galactic tidal field. Our results therefore support the suggestion that at least some of the star clusters formed in merging galaxies can be regarded as young globular clusters. Further investigations of these objects may shed light on the processes by which old globular clusters formed.

We thank Howard Bond, Kenneth Freeman, Douglas Heggie, Massimo Stiavelli, Bradley Whitmore, Chun Xu, and an anonymous referee for helpful discussions and correspondence. This work was supported in part by the National Aeronautics and Space Administration through grant number GO-07468 from the Space Telescope Science Institute and by the National Science Foundation through grant number PHY94-07194 to the Institute for Theoretical Physics.

A. Adiabatic Correction Factors

In this appendix, we present approximate expressions for the average adiabatic corrections to the energy changes within a cluster (relative to those for an impulsive response). This is important because the stars in the inner region of a cluster may respond nearly adiabatically to a gravitational shock, while those in the outer region may respond nearly impulsively. The local adiabatic correction factors for first- and second-order energy changes, $A_1(x)$ and $A_2(x)$, are usually regarded as functions of the dimensionless variable $x = \omega(r)\tau_{sh}$, where $\omega(r)$ is the orbital angular frequency at a radius r within the cluster, $\tau_{sh} = H/V_Z$ is the effective duration of the shock, and H is the scale height of the disk. Since these energy changes are caused by tidal accelerations, they are proportional to r^2 . Thus, the mass-weighted average adiabatic correction factors for first- and second-order changes in the total energy of a cluster are given by

$$\bar{A}_{1,2} = \frac{\int_0^{r_t} r^2 A_{1,2}[x(r)] \rho(r) r^2 dr}{\int_0^{r_t} r^2 \rho(r) r^2 dr}. \quad (\text{A1})$$

We compute $\bar{A}_{1,2}$ from equation (A1) with the following approximations. Several formulae have been proposed for the local adiabatic correction factors (see Gnedin et al. 1999 for a summary). We adopt the limiting form derived by Weinberg (1994) from linear perturbation theory:

$$A_1(x) = A_2(x) = (1 + x^2)^{-3/2}. \quad (\text{A2})$$

This approximates the results of N-body simulations for slow shocks. Similar expressions, but with more negative exponents, apply for fast shocks (Gnedin & Ostriker 1999). The errors we introduce by using equation (A2) in both cases are acceptably small since A_1 and A_2 both approach 1 for fast shocks.

The effects of gravitational shocks are greatest at large radii ($x \lesssim 1$), where the internal potential of a cluster, usually very centrally concentrated, is nearly Keplerian. Thus, we approximate

the orbital angular frequency by the formula

$$\omega(r) = \left(\frac{r}{r_t} \right)^{-3/2} \left(\frac{GM}{r_t^3} \right)^{1/2}. \quad (\text{A3})$$

This is exact for circular orbits near the tidal radius. The coefficient in equation (A3) would be larger for radial orbits with apocenters near r_t ($\sqrt{2}$ rather than 1), but the stars would then spend much of their time at smaller radii [rms radius = $(5/8)^{1/2}r_t$]. These effects largely cancel, indicating that equation (A3) is approximately valid for most stars in the outer region of a cluster (where A_1 and A_2 are non-negligible).

Finally, in the numerical integrations of equation (A1), we approximate the density profile of the clusters by the simple formula

$$\rho(r) \propto \frac{1}{r^2} \left(1 - \frac{r}{r_t} \right)^{5/2}. \quad (\text{A4})$$

In the outer region, this matches the profile of the King (1966) model, $\rho(r) \propto (1/r - 1/r_t)^{5/2}$ for $r \rightarrow r_t$. Furthermore, in the inner region, it has the singular behavior appropriate for core collapse models, $\rho(r) \propto r^{-2}$ for $r \rightarrow 0$ (Spitzer 1987). The half-mass radius of our model is $r_h = 0.18r_t$, reasonably close to that of the Hénon (1961) model ($r_h = 0.15r_t$). Figure 12 shows the resulting average adiabatic correction factor, $\bar{A} = \bar{A}_1 = \bar{A}_2$, as a function of the dimensionless variable

$$x_t \equiv \omega(r_t)\tau_{sh} = (4\pi G \bar{\rho}/3)^{1/2} (H/V_Z). \quad (\text{A5})$$

This depends on E and J through $\bar{\rho}$ [see equations (14) and (15)] and on J , R , and θ through V_Z [see equation (20)]. We adopt $H = 260$ pc in all our calculations (Binney & Merrifield 1998).

B. Distribution of Pericenters

In this appendix, we derive expressions for the density of pericenter distances $n(R_p)$ from the distribution function $f(E, J)$, the density of clusters in position-velocity space with orbital energies and angular momenta near E and J . To do so, we introduce the auxiliary function $N(E, J)$, defined such that $N(E, J)dEdJ$ is the number of clusters with energies and angular momenta in the small intervals $(E, E + dE)$ and $(J, J + dJ)$. Then the number of clusters with pericenters in the interval $(R_p, R_p + dR_p)$ is given by

$$4\pi R_p^2 n(R_p)dR_p = \int_{R_p V_c}^{\infty} N[E(R_p, J), J] \left| \left(\frac{\partial E}{\partial R_p} \right)_J \right| dJ dR_p, \quad (\text{B1})$$

where $E(R_p, J)$ is the energy of an orbit with pericenter R_p and angular momentum J . Using equation (14) and the relation $N(E, J) = 8\pi^2 J f(E, J) P_R(E, J)$ (see equation 2-89 of Spitzer 1987), where $P_R(E, J)$ is the radial period defined in equation (17), we obtain

$$n(R_p) = \frac{2\pi}{R_p^3} \int_{R_p V_c}^{\infty} J f[E(R_p, J), J] P_R[E(R_p, J), J] [(J/R_p)^2 - V_c^2(R_p)] dJ. \quad (\text{B2})$$

As in the main text, we assume the galaxy has a logarithmic potential, with $V_c = \text{const.}$ Then, for the Eddington initial distribution function, we obtain

$$n_0(R_p) \propto \pi V_c^3 R_p^{-\gamma} \int_1^\infty \exp(-\frac{1}{2}\gamma x[1 + (R_p/R_A)^2]) I(x)(x-1) dx, \quad (\text{B3})$$

and for the scale-free initial distribution function

$$n_0(R_p) \propto \pi V_c^{3-2\beta} R_p^{-2\beta-\gamma} \int_1^\infty \exp(-\frac{1}{2}\gamma x)x^{-\beta} I(x)(x-1) dx. \quad (\text{B4})$$

Here, we have changed the variable of integration from J to $x = (J/R_p V_c)^2$ and introduced the parameter $\gamma = (V_c/\sigma)^2$ (as before) and the function

$$I(x) = \int_1^{y(x)} [x(z-1) - z \ln z]^{-1/2} dz, \quad (\text{B5})$$

where $y(x)$ is the upper root of the equation

$$x(y-1) = y \ln y. \quad (\text{B6})$$

In Figure 13, we plot the initial density of pericenters $n_0(R_p)$, along with the initial density of cluster positions $n_0(R)$, for both the Eddington and scale-free initial distribution functions with the standard values of the parameters ($\gamma = 2.5$ and $R_A = 5$ kpc for the former, $\gamma = 3.5$ and $\beta = 0.5$ for the latter). This shows the important result that, for the Eddington model, the distribution of pericenters is narrower than the distribution of cluster positions, while for the scale-free model, the distributions of pericenters and cluster positions have the same power-law form. Consequently, there is less radial variation in the disruption rates for the Eddington distribution function than for the scale-free distribution function.

REFERENCES

Aguilar, L., Hut, P., & Ostriker, J. P. 1988, ApJ, 335, 720
 Baumgardt, H. 1998, A&A, 330, 480
 Bell, E. F., & de Jong, R. S. 2001, ApJ, 550, 212
 Binney, J., & Merrifield, M. 1998, Galactic Astronomy (Princeton: Princeton Univ. Press)
 Binney, J., & Tremaine, S. 1987, Galactic Dynamics (Princeton: Princeton Univ. Press)
 Caputo, F., & Castellani, V. 1984, MNRAS, 207, 185
 Chaboyer, B., Demarque, P., Kernan, P. J., & Krauss, L. M. 1998, ApJ, 494, 96
 Chernoff, D. F., Kochanek, C. S., & Shapiro, S. L. 1986, ApJ, 309, 183

Chernoff, D. F., & Shapiro, S. L. 1987, *ApJ*, 322, 113

Chernoff, D. F., & Weinberg, M. D. 1990, *ApJ*, 351, 121

Christian, C. A., & Schommer, R. A. 1988, *AJ*, 95, 704

Dickey, J. M., & Garwood, R. W. 1989, *ApJ*, 341, 201

Dinescu, D. I., Girard, T. M., & van Altena, W. F. 1999, *AJ*, 117, 1792

Elmegreen, B. G., & Efremov, Y. N. 1997, *ApJ*, 480, 235

Elson, R. A. W., & Fall, S. M. 1985, *PASP*, 97, 692

Fall, S. M., & Rees, M. J. 1977, *MNRAS*, 181, 37P

———. 1985, *ApJ*, 298, 18

Frenk, C. S., & White, S. D. M. 1980, *MNRAS*, 193, 295

Fritze-von Alvensleben, U. 1999, *A&A*, 342, L25

Fukushige, T., & Heggie, D. C. 1995, *MNRAS*, 276, 206

Gnedin, O. Y., Lee, H. M., & Ostriker, J. P. 1999, *ApJ*, 522, 935

Gnedin, O. Y., & Ostriker, J. P. 1997, *ApJ*, 474, 223

———. 1999, *ApJ*, 513, 626

Gratton, R. G., Fusi Pecci, F., Carretta, E., Clementini, G., Corsi, C. E., & Lattanzi, M. 1997, *ApJ*, 491, 749

Harris, W. E. 1991, *ARA&A*, 29, 543

———. 1996, *AJ*, 112, 1487

———. 1999, <http://www.physics.mcmaster.ca/Globular.html> (revision of June 22, 1999)

Hénon, M. 1961, *Ann. d'Astrophys.*, 24, 369

Hut, P., & Djorgovski, S. 1992, *Nature*, 359, 806

Innanen, K. A., Harris, W. E., & Webbink, R. F. 1983, *AJ*, 88, 338

Johnstone, D. 1993, *AJ*, 105, 155

Kang, H., Shapiro, P. R., Fall, S. M., & Rees, M. J. 1990, *ApJ*, 363, 488

King, I. R. 1962, *AJ*, 67, 471

———. 1966, AJ, 71, 64

Kundić, T., & Ostriker, J. P. 1995, ApJ, 438, 702

Lee, H. M., & Goodman, J. 1995, ApJ, 443, 109

Lee, H. M., & Ostriker, J. P. 1987, ApJ, 322, 123

Leitherer, C., Schaerer, D., Goldader, J. D., González Delgado, R. M., Robert, C., Foo Kune, D., de Mello, D. F., Devost, D., & Heckman, T. M. 1999, ApJS, 123, 3

McLaughlin, D. E. 1994, PASP, 106, 47

Meurer, G. R. 1995, Nature, 375, 742

Murali, C., & Weinberg, M. D. 1997a, MNRAS, 288, 749

———. 1997b, MNRAS, 288, 767

———. 1997c, MNRAS, 291, 717

Okazaki, T., & Tosa, M. 1995, MNRAS, 274, 48

Ostriker, J. P., & Gnedin, O. Y. 1997, ApJ, 487, 667

Ostriker, J. P., Spitzer, L., & Chevalier, R. A. 1972, ApJ, 176, L51

Reid, I. N. 1997, AJ, 114, 161

Solomon, P. M., & Rivolo, A. R. 1989, ApJ, 339, 919

Spitzer, L. 1987, *Dynamical Evolution of Globular Clusters* (Princeton: Princeton Univ. Press)

Spitzer, L., & Chevalier, R. A. 1973, ApJ, 183, 565

van den Bergh, S., & Lafontaine, A. 1984, AJ, 89, 1822

Vesperini, E. 1997, MNRAS, 287, 915

———. 1998, MNRAS, 299, 1019

———. 2000, MNRAS, 318, 841

———. 2001, MNRAS, 322, 247

Vesperini, E., & Heggie, D. C. 1997, MNRAS, 289, 898

Weinberg, M. D. 1994, AJ, 108, 1403

Whitmore, B. C. 1997, in *The Extragalactic Distance Scale*, ed. M. Livio, M. Donahue, & N. Panagia (Cambridge: Cambridge Univ. Press), 254

Whitmore, B. C., Zhang, Q., Leitherer, C., Fall, S. M., Schweizer, F., & Miller, B. W. 1999, AJ, 118, 1551

Zhang, Q., & Fall, S. M. 1999, ApJ, 527, L81

Zinn, R. 1985, ApJ, 293, 424

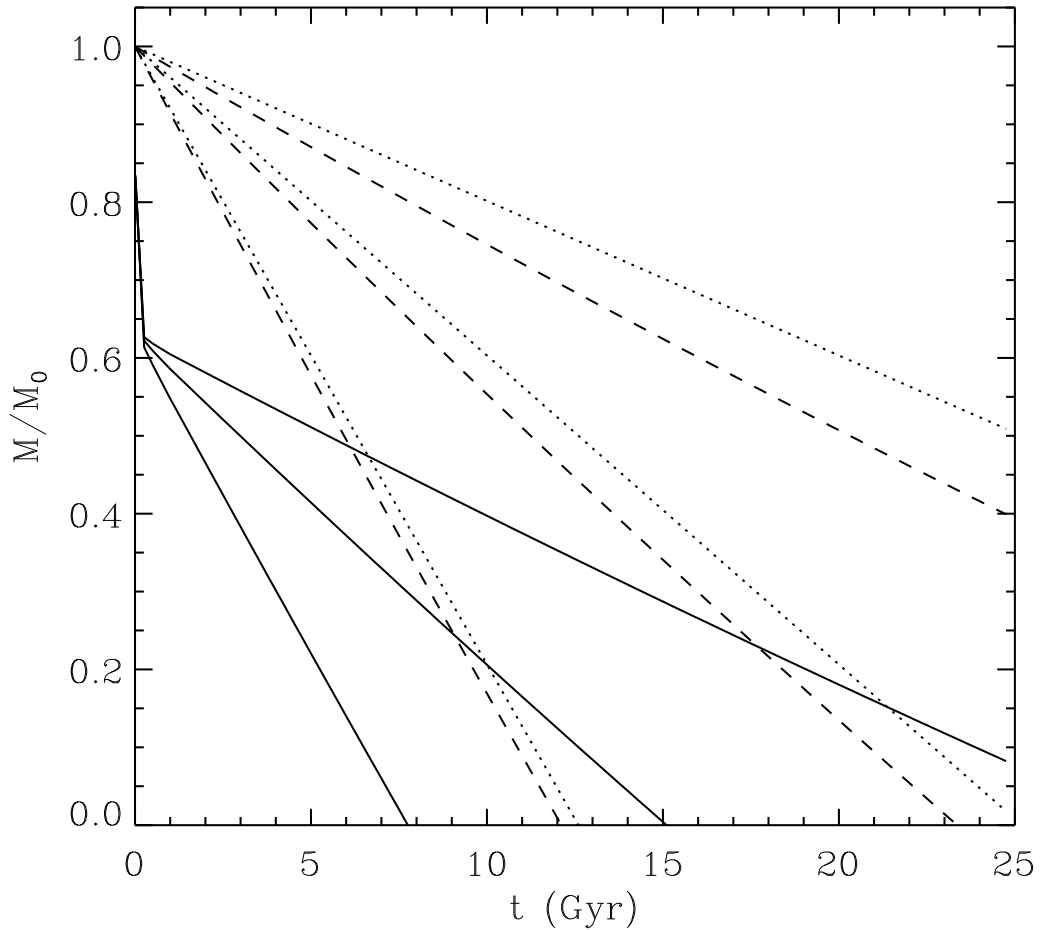


Fig. 1.— Evolution of the masses of clusters predicted by equations (7)–(10) with three different initial masses: $M_0 = (1, 2, 4) \times 10^5 M_\odot$. All three clusters have the same orbit, with $R_p = 4$ kpc, $R_a = 6$ kpc, and $\theta = 45^\circ$. The dotted lines show the evolution with two-body relaxation alone, the dashed lines with two-body relaxation and gravitational shocks, and the solid lines with two-body relaxation, gravitational shocks, and stellar evolution. Note that stellar evolution dominates in the early stages, that gravitational shocks become relatively less important as the mass decreases, and that two-body relaxation dominates in the late stages.

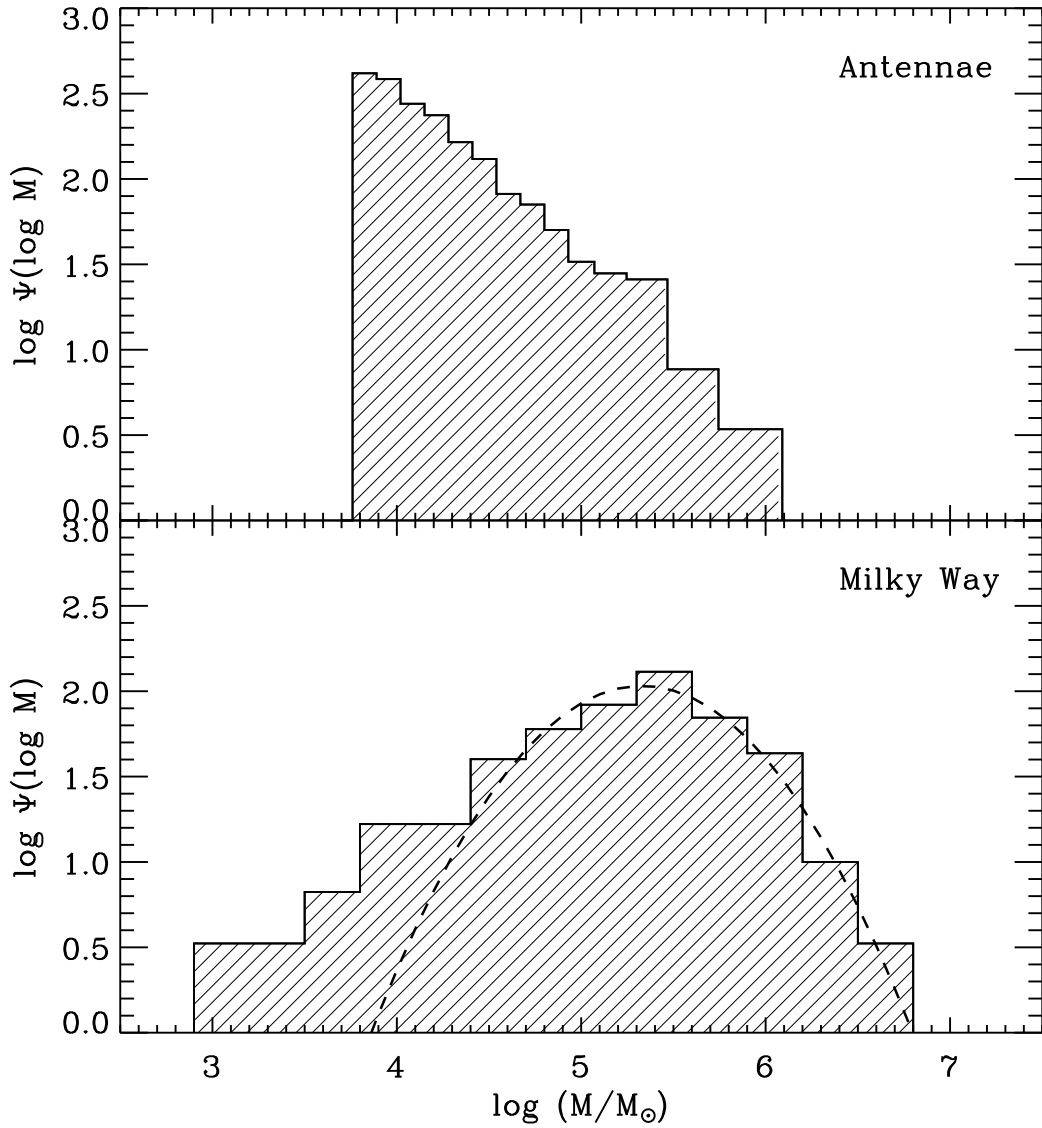


Fig. 2.— Histograms of the masses of young star clusters in the Antennae galaxies and old globular clusters in the Milky Way. The former is from Zhang & Fall (1999); the latter is based on data compiled by Harris (1996, 1999). Note that the mass function of the young clusters declines monotonically over the entire observed range, $\log(M/M_\odot) > 3.8$, whereas the mass function of the old clusters rises to a peak and then declines. The dashed curve is the usual lognormal representation of the mass function with $M_p = 2 \times 10^5 M_\odot$ and $\sigma(\log M) = 0.5$, corresponding to a Gaussian distribution of absolute magnitudes with $\langle M_V \rangle = -7.3$ and $\sigma(M_V) = 1.2$ (for $M/L_V = 3$). Note that the empirical mass function of the old clusters (histogram) is shallower below the peak than the lognormal function.

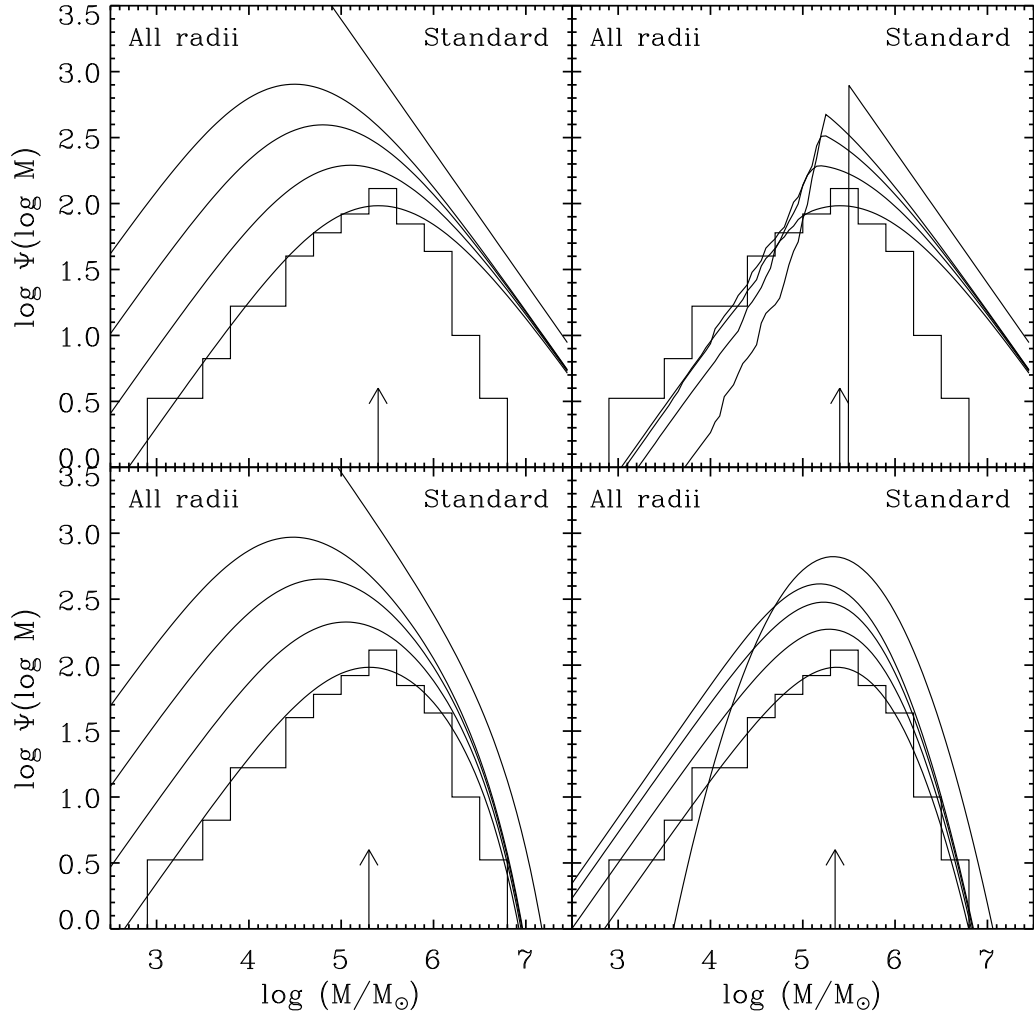


Fig. 3.— Evolution of the mass function, averaged over all radii, for the Eddington initial distribution function with the standard parameters and different initial mass functions. These are: a power law of index $\beta = -2$ (top left), the same power law truncated at $3 \times 10^5 M_\odot$ (top right), a Schechter function with $\beta = -2$ and $M_* = 5 \times 10^6 M_\odot$ (bottom left), a lognormal function with $M_p = 2 \times 10^5 M_\odot$ and $\sigma(\log M) = 0.5$ (bottom right). Each mass function is plotted at $t = 0, 1.5, 3, 6$, and 12 Gyr; the arrows indicate the peak at $t = 12$ Gyr. The histograms depict the empirical mass function of globular clusters in the Milky Way. Note that the peak mass in the models is similar to that in the observations for the four different initial conditions.

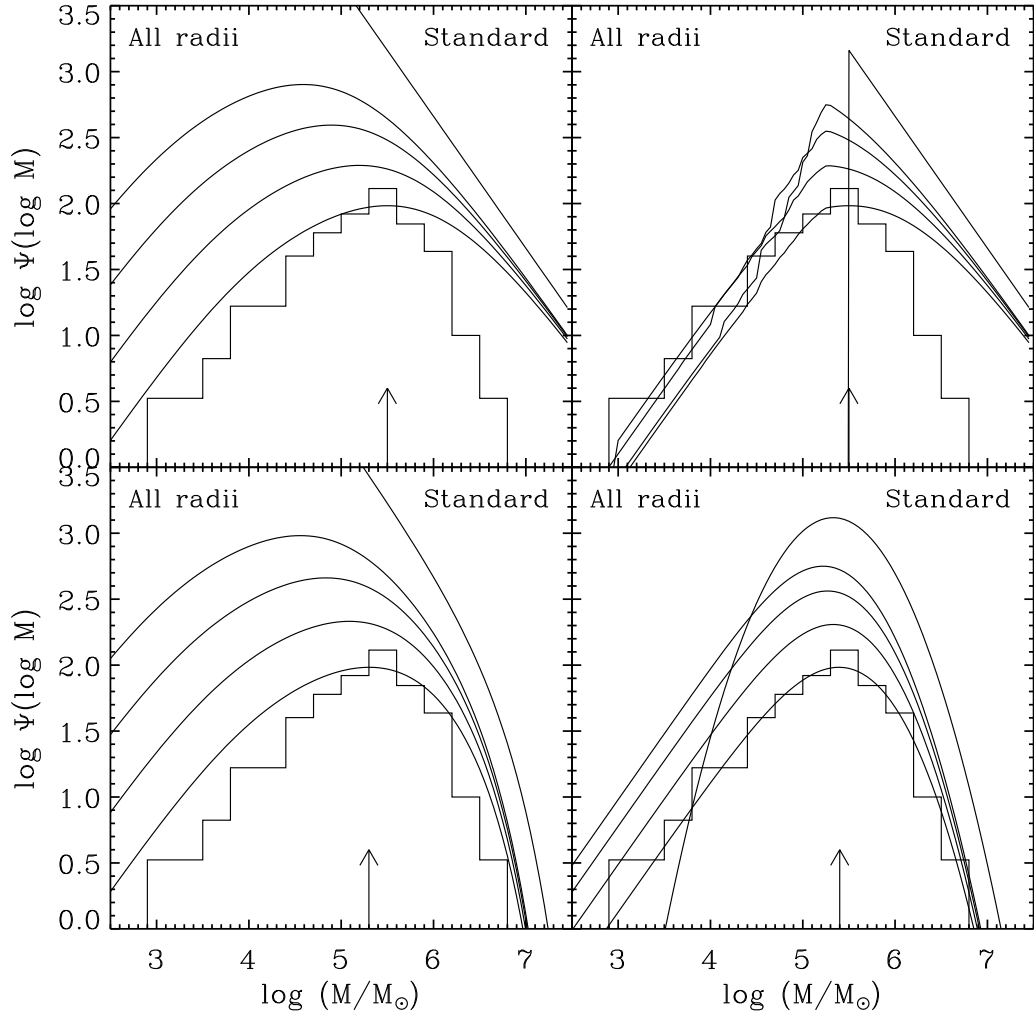


Fig. 4.— Evolution of the mass function, averaged over all radii, for the scale-free initial distribution function with the standard parameters and different initial mass functions. These are: a power law of index $\beta = -2$ (*top left*), the same power law truncated at $3 \times 10^5 M_\odot$ (*top right*), a Schechter function with $\beta = -2$ and $M_* = 5 \times 10^6 M_\odot$ (*bottom left*), a lognormal function with $M_p = 2 \times 10^5 M_\odot$ and $\sigma(\log M) = 0.5$ (*bottom right*). Each mass function is plotted at $t = 0, 1.5, 3, 6$, and 12 Gyr; the arrows indicate the peak at $t = 12$ Gyr. The histograms depict the empirical mass function of globular clusters in the Milky Way. Note that the peak mass in the models is similar to that in the observations for the four different initial conditions.

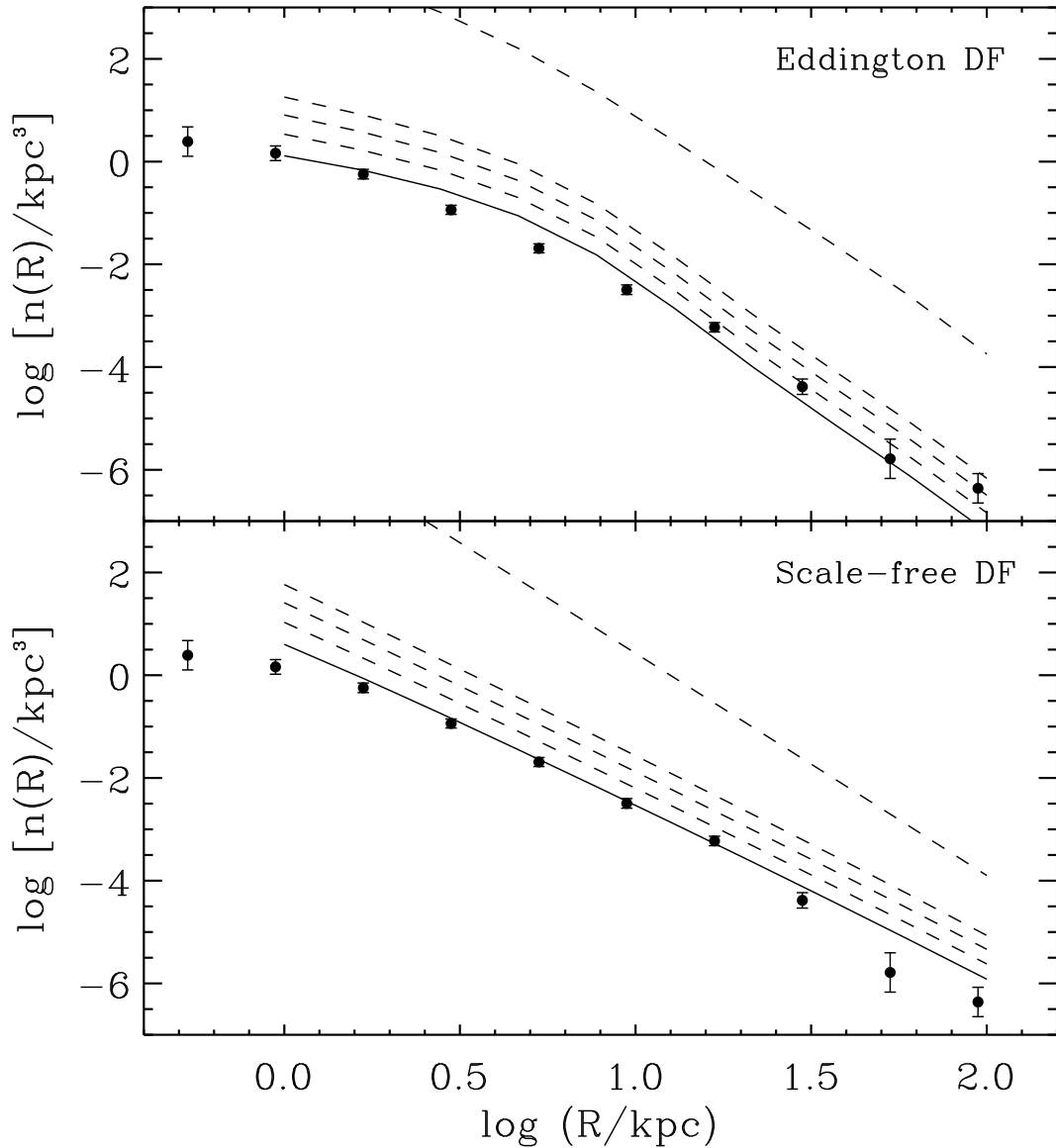


Fig. 5.— Evolution of the number density profile of the cluster system for the Eddington and scale-free initial distribution functions with the standard parameters and the Schechter initial mass function. The profiles are plotted at $t = 0, 1.5, 3, 6$, and 12 Gyr. To avoid a divergence in the initial density profile, the mass function is truncated at $100 M_\odot$. The data points depict the empirical profile for globular clusters in the Milky Way. Note that the final profiles in the models are in reasonable agreement with the empirical profile.

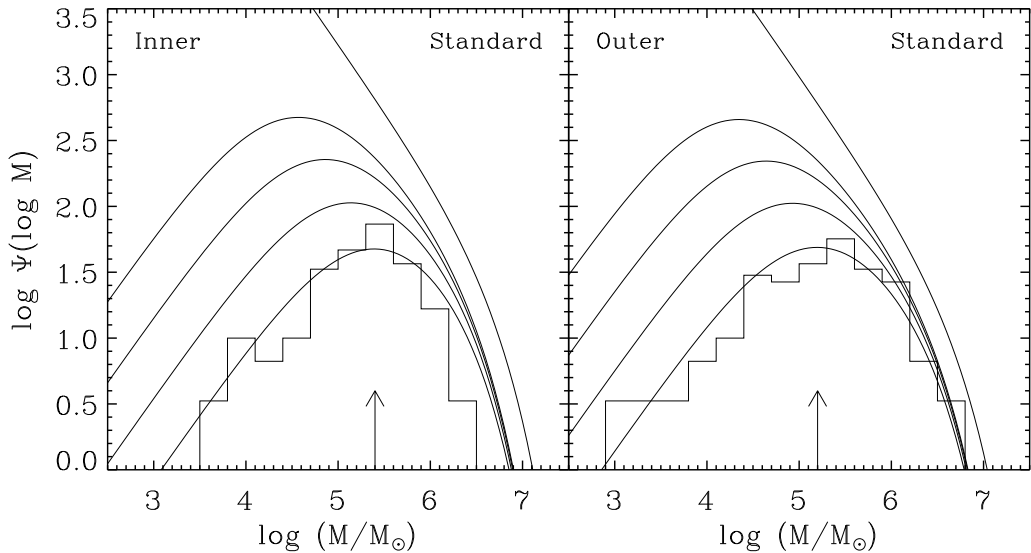


Fig. 6.— Evolution of the mass function, averaged over inner radii ($R < 5$ kpc) and outer radii ($R > 5$ kpc), for the Eddington initial distribution function with the standard parameters and the Schechter initial mass function. Each mass function is plotted at $t = 0, 1.5, 3, 6$, and 12 Gyr; the arrows indicate the peak at $t = 12$ Gyr. The histograms depict the empirical mass functions of globular clusters in the Milky Way in the corresponding ranges of radii. Note that the shift in the peak mass in the models between inner and outer radii is relatively small.

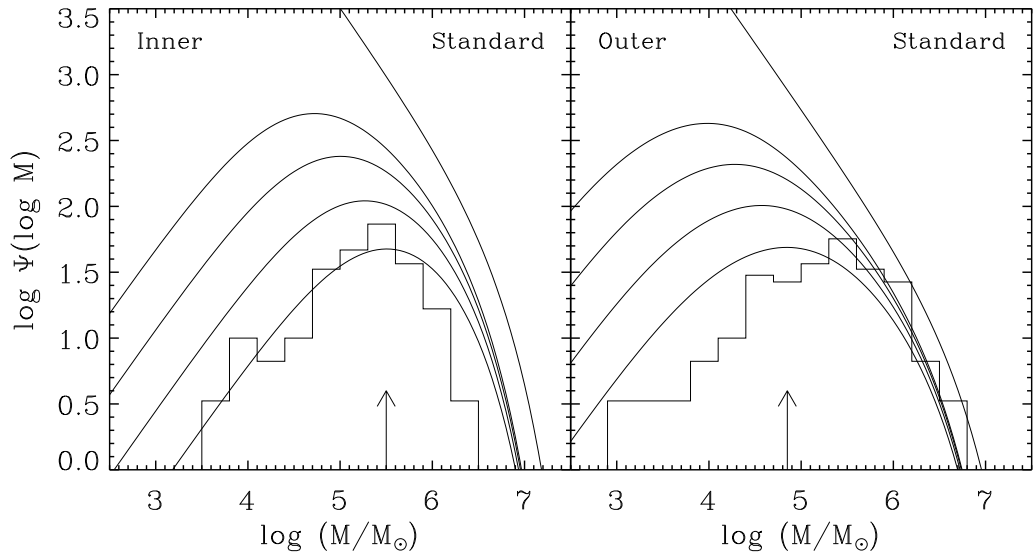


Fig. 7.— Evolution of the mass function, averaged over inner radii ($R < 5$ kpc) and outer radii ($R > 5$ kpc), for the scale-free initial distribution function with the standard parameters and the Schechter initial mass function. Each mass function is plotted at $t = 0, 1.5, 3, 6$, and 12 Gyr; the arrows indicate the peak at $t = 12$ Gyr. The histograms depict the empirical mass functions of globular clusters in the Milky Way in the corresponding ranges of radii. Note that the shift in the peak mass in the models between inner and outer radii is relatively large.

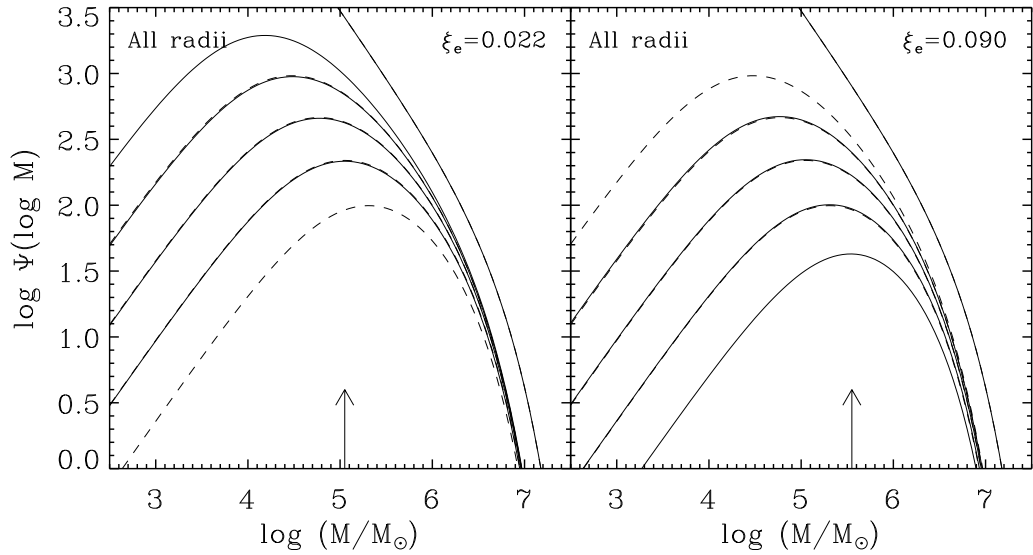


Fig. 8.— Evolution of the mass function, averaged over all radii, with different values of the escape probability parameter ξ_e (as indicated), for the Eddington initial distribution function and the Schechter initial mass function. Each mass function is plotted at $t = 0, 1.5, 3, 6$, and 12 Gyr; the arrows indicate the peak at $t = 12$ Gyr. The dashed curves represent the same models with the standard parameters. Note that the peak mass in the models is larger for larger ξ_e .

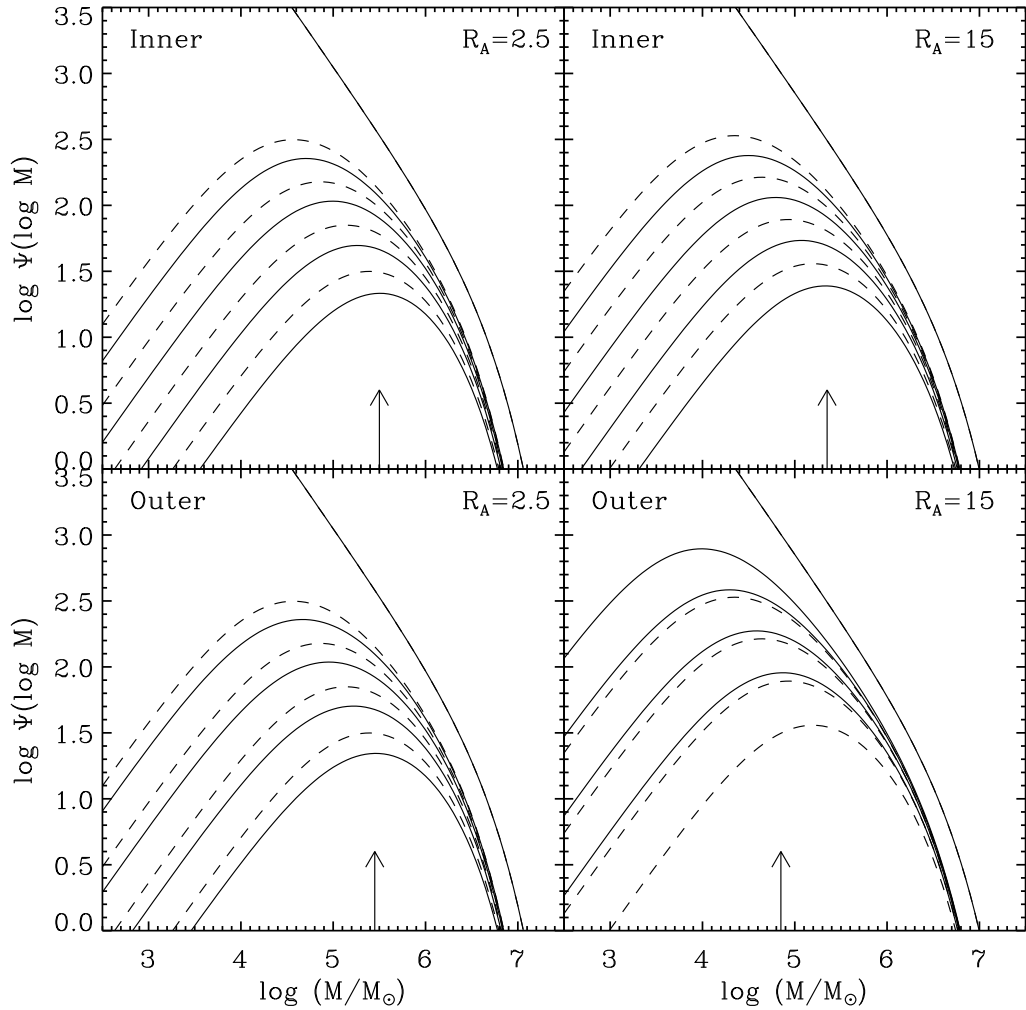


Fig. 9.— Evolution of the mass function, averaged over inner radii ($R < 5$ kpc) and outer radii ($R > 5$ kpc), with different values of the velocity anisotropy radius R_A (in kpc, as indicated), for the Eddington initial distribution function and the Schechter initial mass function. Each mass function is plotted at $t = 0, 1.5, 3, 6$, and 12 Gyr; the arrows indicate the peak at $t = 12$ Gyr. The dashed curves represent the same models with the standard parameters. Note that the shift in the peak mass in the models between inner and outer radii is larger for larger R_A .

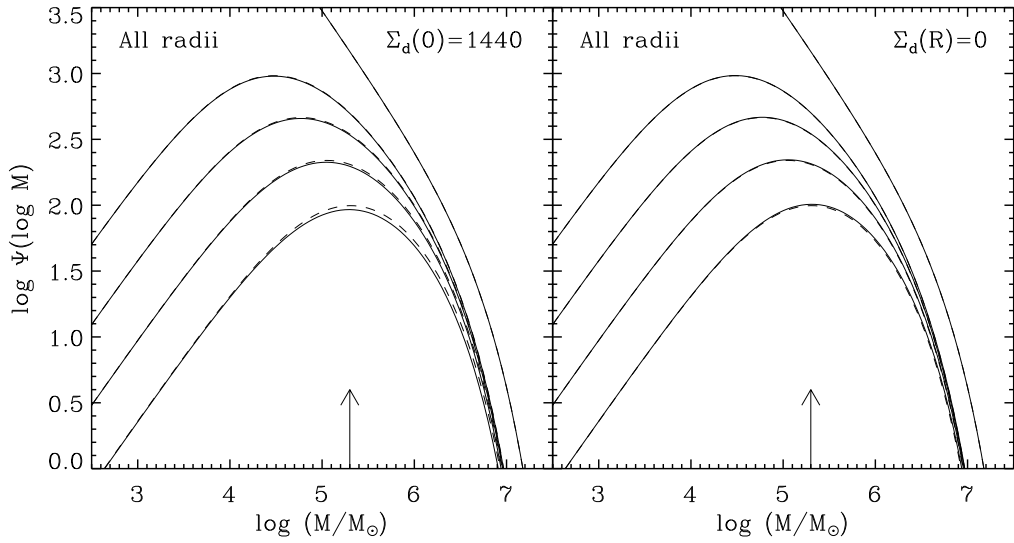


Fig. 10.— Evolution of the mass function, averaged over all radii, with a more massive exponential disk (*left panel*) and with no disk (*right panel*), for the Eddington initial distribution function and the Schechter initial mass function. Each mass function is plotted at $t = 0, 1.5, 3, 6$, and 12 Gyr; the arrows indicate the peak at $t = 12$ Gyr. The dashed curves represent the same models with the standard parameters. Note that the peak mass in the models is smaller for stronger disks.

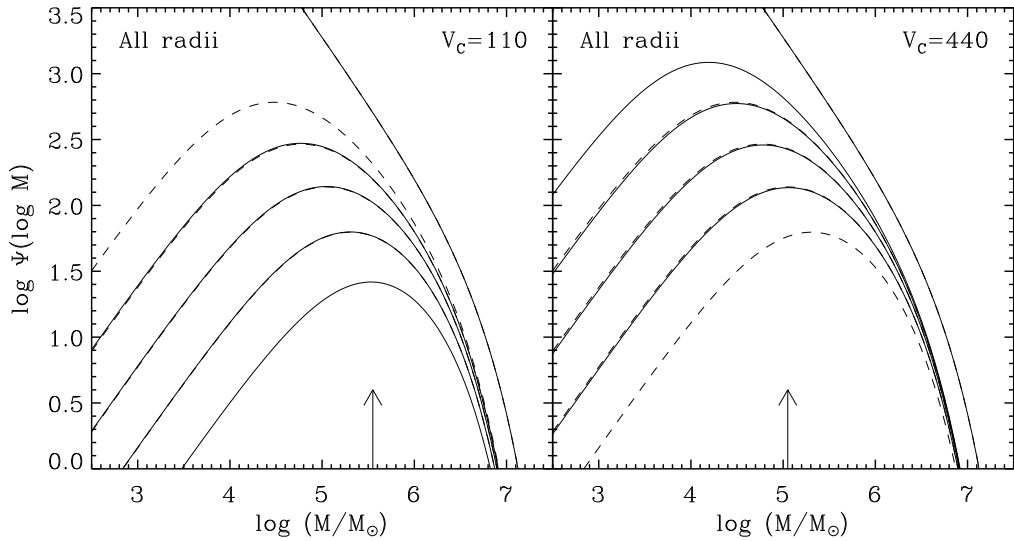


Fig. 11.— Evolution of the mass function, averaged over all radii, with different values of the circular velocity V_c (in km s^{-1} , as indicated), for the Eddington initial distribution function and the Schechter initial mass function, and for $k = 4$ in the relation $M_g \propto V_c^k$. Each mass function is plotted at $t = 0, 1.5, 3, 6$, and 12 Gyr ; the arrows indicate the peak at $t = 12 \text{ Gyr}$. The dashed curves represent the same models with the standard parameters. For $k < 4$, the mass function has a weaker dependence on V_c than shown here (as explained in the text).

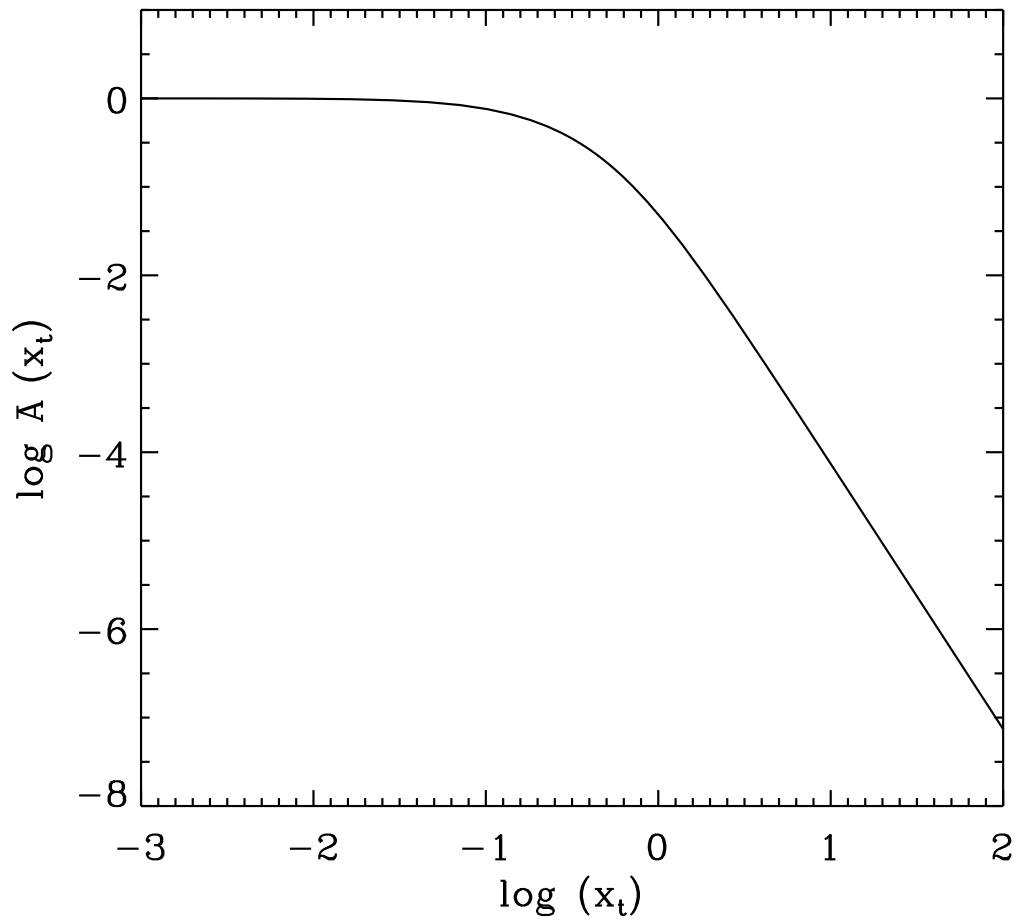


Fig. 12.— Average adiabatic correction factor for first- and second-order changes in the total energy of a cluster plotted against the dimensionless variable $x_t = \omega(r_t)\tau_{sh}$. See Appendix A for details.

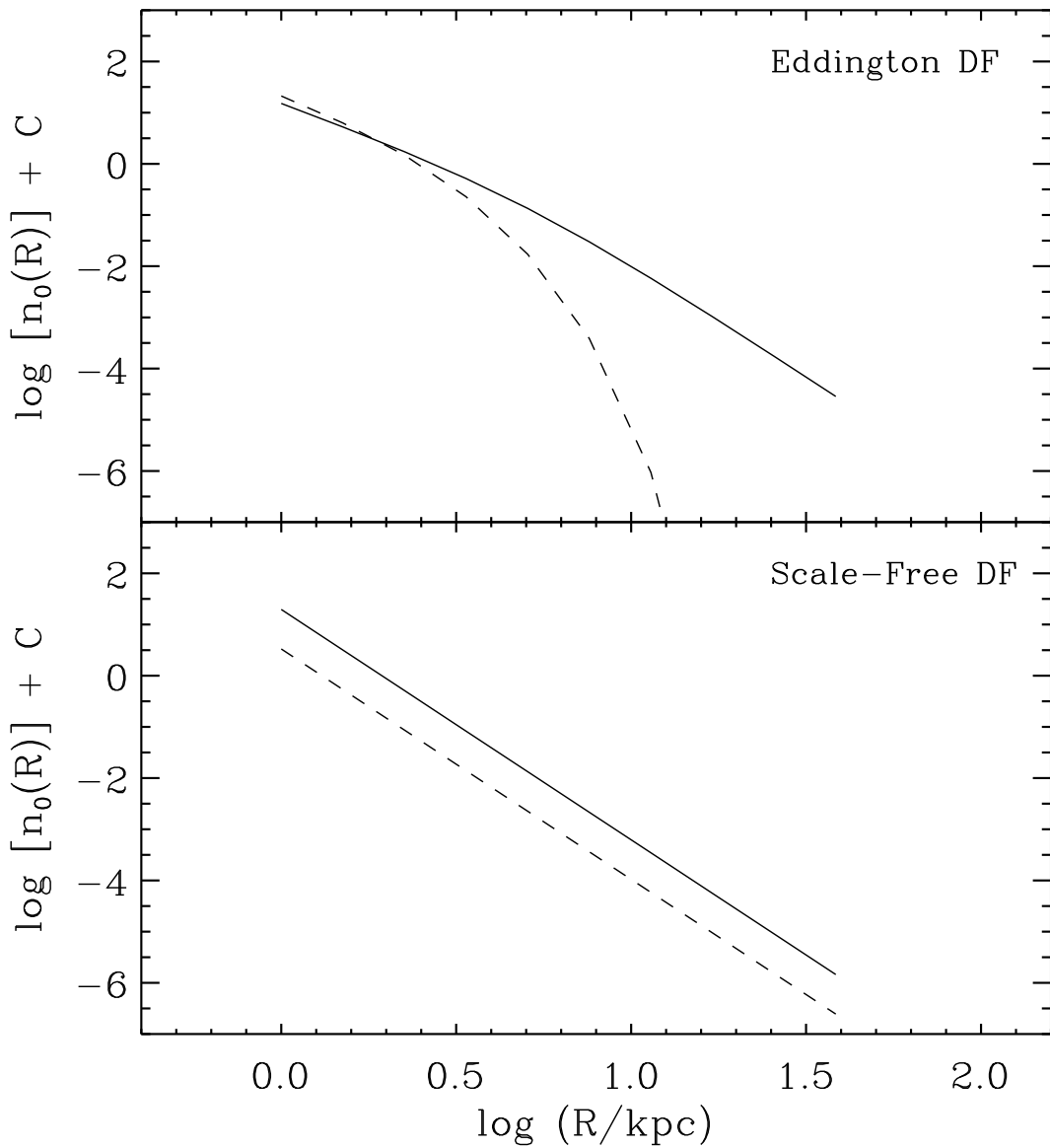


Fig. 13.— Initial densities of cluster positions (solid lines) and pericenters (dashed lines) for the Eddington and scale-free distribution functions. Note that the distribution of pericenters is narrower than the distribution of cluster positions for the Eddington model but not for the scale-free model.

Table 1. Present Total Disruption Rates and Survival Fractions

Initial Mass Function	$ \dot{N}_T/N_T ^a$	$ \dot{M}_T/M_T ^a$	$N_T/N_{T0})^b$	$M_T/M_{T0})^b$
Power Law	0.064	0.022	0.00–0.02	0.08–0.19
Truncated Power Law	0.051	0.021	0.47	0.37
Schechter	0.079	0.049	0.00–0.01	0.04–0.10
Lognormal	0.072	0.057	0.17	0.16

^aRates are in Gyr^{−1}.

^bRanges are for a lower cutoff in $\psi_0(M)$ from $M_l = 1 M_\odot$ to $10^4 M_\odot$.